Correlation and Prediction of Mass Transport across Membranes I: Influence of Alkyl Chain Length on Flux-Determining Properties of Barrier and Diffusant

G. L. FLYNN[▲] and S. H. YALKOWSKY

Abstract ☐ The effect of alkyl chain length on the physicochemical properties of a series of *p*-aminobenzoate esters, determinant of the rate at which they penetrate inert barriers, was investigated. Relationships are drawn for the influence of chain length on partition coefficient and solubility; and these, in conjunction with a diffusion layer membrane model, have been incorporated into a general, theoretical expression for maximum steady-state flux as a function of homolog size. This expression predicts a parabolic dependency as the homologous series is ascended for certain reasonably normal conditions. This model was tested and found valid for an uninterrupted ester series containing from one to seven carbons, utilizing dimethylpolysiloxane membranes. An analysis of the effect of each parameter in the equation was performed with computer assistance. This analysis shows the extent to which the optimum chain length for absorption (barrier penetration) is dependent on controllable and uncontrollable experimental factors. The broad applications of the diffusion layer membrane model with superimposed solubility constraints for the interpretation of membrane transport phenomena, including bioavailability, are detailed.

Keyphrases ☐ Membrane diffusion—maximum steady-state flux as a function of homolog size, alkyl *p*-aminobenzoates ☐ Chain length effect—membrane diffusion of alkyl *p*-aminobenzoates ☐ Alkyl *p*-aminobenzoates—effect of chain length on membrane diffusion ☐ Homologous alkyl series, *p*-aminobenzoates—effect of chain length on membrane diffusion ☐ Structure-activity relationships—effect of alkyl chain length on membrane diffusion, *p*-aminobenzoate esters

In a very real sense, progress in biopharmaceutics is limited by contemporary understanding of the processes governing drug absorbability and biodistributivity. For the most part, current physicochemical models applicable to these processes are simplistic and take into account only partition coefficient and membrane diffusivity as the absorption- and distribution-determining factors. Newly emerging models are necessarily more complex and comprehensive. They are also quite comprehensible (1–3). In addition to the standard factors, these models consider the significance of the solvent diffusion layers and the substrate diffusivities therein. The model presented here superimposes one additional factor, the aqueous solubility of the diffusant. All in all, this approach should provide the medicinal chemist a feel for the biological effects of his chemical manipulations, the pharmacologist some basis for separating nonspecific effects from those individualized with respect to the receptor, and the physician a better understanding of relative potency and side effects of structurally related compounds.

Requisite to developing the concepts put forth here was the selection of a membrane requiring a partitioning step (rather than pore permeation or dialysis) and having generally high diffusant mobility (diffusivity). Dimethylpolysiloxane seemed an ideal material. The earliest investigations of this silicone rubber [notably Barrer *et al.* (4) and Barrer and Chio (5)] showed it to be extremely permeable to a variety of gases. This permeability is attributable to large diffusivities resulting from noncrystallinity at ambient temperature and high segmental motility.

The first studies in which dimethylpolysiloxane sheeting was used to simulate drug absorption processes were by Garrett and Chemburkar (6–8) who demonstrated facile permeability of several drug species. Nakano and Patel (9) extended this work, studying mechanisms by which complexing agents influence drug transport. These investigators did not differentiate between diffusive and partitioning contributions to relative permeability. Studies by Haleblian *et al.* (10), Most (11), Flynn and Roseman (12), and Flynn and Smith (13) are therefore notable, because they contain such fundamental information for steroids and several other compounds. Other investigators provided referable data obtained with related dimethylpolysiloxane systems such as capsules, implants, and vaginal rings. Steroid release studies of Roseman and Higuchi (14) and Roseman (15) are important, since these authors recognized the contribution of diffusion layers to the overall release pattern. Only after an earlier drug release equation (16) was amended to account for diffusion layer involvement were they able to interpret mathematically their release profiles.

Appreciation of the role played by diffusion layers in barrier permeation is increasing. Zwolinski *et al.* (17) pointed to this factor in a foresighted article on the penetration of biological barriers. More recently, Stehle and Higuchi (1) indicated conditions whereby diffusion layers determine flux. Similarly, Beck and Schultz (18) dealt with this problem in measuring hindered diffusion through microporous mica sheets. The biological importance of diffusion layers has not gone undetected. They have been shown to influence sodium and potassium penetration of frog skin (19). Cuthbert and Dunant (20) demonstrated that the rate of diffusion through the immobile solvent layer can even govern the time course of cellular responses. Ho and Higuchi (3) re-

Table I—Conditions and Yields for Preparation of *p*-Nitrobenzoates

p-Nitrobenzoate	Molecular Weight	*p*-Nitrobenzoyl Chloride, g.	Respective Alcohol, g.	Crude Yield[a], g.	Boiling-Point Range, Distillation Fraction	Pressure of Distillation, mm.
Propyl[b]	209	40.0	12.95	39.4	143–146°	2.2
Butyl	223	44.0	16.0	41.3	143–146°	1.8
Pentyl	237	44.0	19.0	36.3	148–152°	1.0
Hexyl	251	44.0	22.0	40.0	160–163°	0.8
Heptyl	265	44.0	25.0	47.8	183	2.0
Octyl	279	44.0	28.0	50.0	190°	2.0
Nonyl	293	44.0	31.1	47.0	190°	2.0
Dodecyl	335	44.0	40.2	59.2	—[c]	—[c]
Hexadecyl	391	44.0	57.3	57.8	—[c]	—[c]

[a] Prior to distillation or recrystallization. [b] Prepared in chloroform. [c] Not applicable—recrystallized from warm hexane.

cently presented a fresh treatment of some literature data for buccal absorption, using a diffusion layer–membrane modelistic approach.

The present studies supplement and augment previous investigations. The diffusion layer–membrane model is invoked to explain nonstationary-state and steady-state transfusion of dimethylpolysiloxane membranes by a homologous series of *p*-aminobenzoate esters. *A priori* mathematical expressions for permeation as a function of solubility and partition coefficient, treating the barrier as a laminate, were derived, experimentally tested, and found to describe the phenomena observed adequately.

EXPERIMENTAL[1]

Chemicals—All reagents were used as received. Methyl and ethyl *p*-aminobenzoates were purchased; other esters were synthesized from *p*-nitrobenzoyl chloride and appropriate alcohols[2]. Reagent grade ether[3], chloroform[3], and hexane[4] were used in the crystallizations. Deionized water was used in dilution and sample preparation.

Membranes—The membranes[5] were obtained in several thicknesses, but only the 0.0126 and 0.0476 were employed.

Synthesis of *p*-Aminobenzoates—Both methyl and ethyl *p*-aminobenzoates were available commercially. The remaining *p*-aminobenzoates were prepared using a modified literature procedure (22). In this procedure the alkyl *p*-nitrobenzoates were first prepared and then hydrogenated to obtain the *p*-amino moiety.

The *p*-nitro esters were synthesized by refluxing a 10% excess of *p*-nitrobenzoyl chloride with the respective alcohols. The sole exception to this procedure was for the propyl derivative, which was prepared by adding a stoichiometric amount of *n*-propanol in alcohol-free chloroform slowly to a solution of the acid chloride, also in alcohol-free chloroform. This was refluxed for several hours. In the other syntheses, the mixture of alcohol and acid chloride was heated to a fluid melt (100–150°) and allowed to react until all physical signs of reaction, particularly gas evolution, ceased. The amounts of reagents and reaction conditions are summarized in Table I. The crude esters were dissolved in ether and washed with 10% sodium carbonate until free from *p*-nitrobenzoic acid. The ethereal solution was then washed with water, and the ether was evaporated. The crude ester was purified by distillation (propyl to nonyl) or by crystallization from hexane (dodecyl and hexadecyl).

The *p*-aminobenzoates were obtained from the *p*-nitrobenzoates in virtually 100% yield using a 5% palladium-on-carbon catalyst. The solvent used in all cases was 3A alcohol. The solvent was evaporated from the crude *p*-aminobenzoate, and the residue was taken up in 25 ml. (propyl to octyl) or 50 ml. (nonyl, dodecyl, and hexadecyl) of chloroform. About 300 ml. of room temperature hexane (propyl to heptyl) or boiling hexane (octyl, nonyl, dodecyl, and hexadecyl) was added to the methylene chloride solutions, and the solutions were allowed to stand and cool for over 24 hr. Large crops of pure white crystalline material were obtained in all instances. These were collected on a Büchner funnel, rinsed with chilled hexane, and placed in a desiccator under vacuum for 2–5 days to remove residual solvent. The crystals were stored in a tightly sealed container. Carbon, hydrogen, and nitrogen analyses were in excellent agreement with theory in all cases. The overall yields ranged from about 20 to about 50 g.

Solubility Determination by UV Analysis[6]—A moderate excess of each compound was placed in an appropriately sized stoppered flask (≃1000 ml.), water was added to the capacity of the flask, and the flask was placed in a 37° shaker bath and agitated gently for 6–8 days. An appropriately sized sample (between 1 and 50 ml.) for each ester was removed *via* a warmed, glass-wool-tipped pipet and appropriately diluted for analysis. A minimum dilution of 100% (50–100 ml.) was used to prevent crystallization at ambient temperature. The absorption maximum at 285 nm. was measured and compared with a simultaneously prepared standard. Appropriate pathlength cells were used; 10-cm. pathlength cells were required for the heptyl through nonyl esters.

The standard solutions were prepared by dissolving accurately weighed samples (10 or 1.0 mg.) of each compound in 10 ml. of 95% ethanol. In each case, these were diluted 100-fold with deionized water and assayed using 1- or 10-cm. cells, respectively. In every case the pathlength of the cell used for the standard corresponded to that used for the sample.

GC Procedures[6]—GC was chosen as the principal analytical procedure for both solubility analyses and diffusional studies, because it provided a means of simultaneous separation and quantitation. The following general procedure was employed:

1. The internal standard was dissolved in 100 ml. of carbon disulfide; the amount of internal standard varied from ester to ester. An attempt was made to have its concentration roughly equivalent to the concentration of the reference solution and samples.

[1] Diffusional experiments were performed in a diffusion cell which was described in detail previously (21). UV analyses were accomplished on both Cary 11 and Zeiss DMR 21 recording spectrophotometers. The GC data were obtained on an F & M scientific 402 chromatograph equipped with an Infotronics model CRS-104 digital readout system. Temperature control was obtained with an Aminco thermostated bath (solubility measurements) and/or a Tamson force/suction circulating bath (diffusion studies). Circulation of the donor contents was by means of a New Brunswick Scientific pump, model PA-23. Exact control of the receptor flow was accomplished with an FMI model RRP piston lab pump. Runs were continuously monitored (qualitatively) with a Beckman DB spectrophotometer equipped with a 12.7-cm. (5-in.) recorder. A Buchi rotovapor evaporator was used to remove solvent from extracted samples. Analysis of the diffusional data and development of the theoretical model was facilitated by the use of an IBM model 370 computer.

[2] The sources were: *p*-nitrobenzoyl chloride, Matheson, Coleman and Bell; methyl *p*-aminobenzoate, Eastman; ethyl *p*-aminobenzoate, Aldrich; *n*-propanol, Eastman; *n*-butanol, source unknown; *n*-pentanol, Aldrich; *n*-hexanol, Aldrich; *n*-heptanol, Aldrich; *n*-octanol, Eastman; *n*-nonanol, Aldrich; *n*-dodecanol, Aldrich; *n*-hexadecanol, Eastman; and *p*-aminobenzoic acid, Eastman.

[3] Mallinckrodt.

[4] Eastman.

[5] Silastic sheeting, Dow Corning, Midland, Mich.

[6] Each of the analytical procedures, UV analyses, and GC assays served as an internal check on the data obtained by the other. This was true for permeation studies as well as solubilities.

Table II—GC Conditions Using Flame-Ionization Detection

p-Aminobenzoate	Gas Flow, ml./min. He Carrier	Gas Flow, ml./min. H_2 Carrier	Component Temperature Column	Component Temperature Detector	Sensitivity	Internal Standard	Retention Times, min. Sample	Retention Times, min. Internal Standard
Methyl	50	37	139°	200°	40	Butyl *p*-aminobenzoate	1.21	3.4
Ethyl	60	37	139°	200°	80	Butyl *p*-aminobenzoate	1.6	2.6
Propyl	60	70	152°	215°	40–80	Hexyl *p*-aminobenzoate	1.0	3.3
Butyl	60	35	167°	218°	20	Chloroeicosane	0.8	4.7
Pentyl	65	35	167°	218°	40	Chloroeicosane	1.2	5.25
Hexyl	60	35	167°	218°	20	Chloroeicosane	2.0	5.2
Heptyl	45	37	167°	220°	20	Triphenylmethane	3.2	1.5
Octyl	45	55	198°	232°	20	Tetraphenylmethane	5.5	14
Nonyl	40	40	218°	240°	20	Triphenylbenzene	0.8	4.1
Dodecyl	60	35	225°	245°	20	Triphenylbenzene	3.0	5.5
Hexadecyl	60	35	225°	245°	20	Triphenylbenzene	9.6	5.5

2. The reference solution was prepared by weighing an exact amount of ester gauged to be roughly equivalent to the average sample size and dissolving it in 1 ml. of the internal standard solution.

3. The dried extracts were dissolved in 1 ml. of internal standard solution.

4. Between 0.3 and 0.5 μl. of sample (and reference solution) was injected onto a 1.22-m. (4-ft.), 3-mm. diameter glass column packed with 1% SE-30 silicone rubber on Diatoport S (80–100 mesh).

The internal standard, carrier gas flow, hydrogen gas flow, and column and detector temperatures varied with each ester. The conditions employed are summarized in Table II. A higher ester was employed as the internal standard for the methyl, ethyl, and propyl derivatives. For the other esters, appropriate organic compounds were found. The selection of the internal standard was on a trial-and-error basis. Several were tried with each ester before the ultimate selection was made. Detection in all cases was with flame ionization.

Peak areas were determined automatically by electronic integration. Each sample was injected a minimum of three times and the data were averaged. The amount of compound in each sample was obtained from:

$$\text{mg./sample} = \frac{B_1}{B_2} \times W \qquad \text{(Eq. 1)}$$

where B_1 is the ratio of sample to internal standard area, B_2 is the ratio of reference to internal standard area, and W is the milligrams of drug in the reference. This value, of course, was divided by the milliliters of sample taken in the solubility analyses to obtain solubility in milligrams per milliliter.

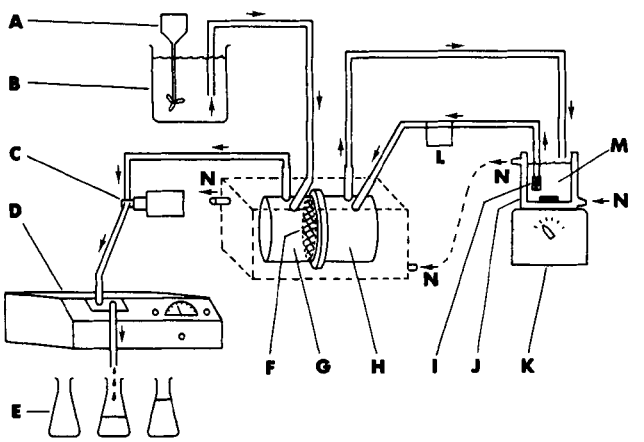

Figure 1—*Schematic of diffusional system. The letters A through G designate the components of the receptor system, namely: A, stirrer; B, 37° reservoir; C, piston pump; D, spectrophotometer with flow cell; E, collecting vessels; F, membrane; and G, receptor compartment. The letters H through M are the donor system components: H, donor compartment; I, filter; J, jacketed reservoir; K, magnetic stirrer; L, tubing pump; and M, saturated (suspension) solution of ester. The N indicates the independent 37° water system for constant temperature.*

Sample and Membrane Preparation—Excess drug was equilibrated at 37° with water for 6–8 days. About 300 ml. of this crude suspension was transferred to the donor reservoir. After circulating the solution through the tubing for roughly 1 hr. with the donor compartment of the cell shunted, the cell was connected and the run commenced. Between 1 and 2 min. was required to fill the donor compartment of the cell since the pumping velocity in this section of the system was between 10 and 20 ml./min. This time was considered negligible considering the prolonged duration of the runs. The receptor cell compartment flush was initiated prior to filling the donor compartment.

Previous experiments indicated that lag times obtained with commercial dimethylpolysiloxane membranes containing silica filler varied and increased as pretreatment (soaking) time in water increased. To standardize this aspect conveniently, membranes were washed with deionized water for exactly 15 min. This was accomplished by fastening the membrane to a stirrer blade with a paper clip and rotating at slow speed for the duration. The membrane was then immediately positioned in the cell and the run was initiated. In every experiment the membrane support screen was placed into the system. This was done to increase effectively the total thickness of the diffusion layers and hasten diffusion layer barrier participation. The significance of this is treated in the *Theoretical* and *Discussion* sections. The sum of the diffusion layer thicknesses in this case was about 200 μm., fully 3–4 times thicker than observed in the absence of the support screen.

Membrane Diffusion Studies—A detailed description of the diffusion cell was presented previously (21). Two studies on other aspects of membrane transport utilizing the diffusion cell were also presented previously (12, 13). As in the case of Flynn and Roseman (12), a donor reservoir was used to ensure that the donor concentration remained constant at saturation. Based on our combined experiences, this was more of a precaution than a requirement, because when water equilibrated with drug and containing excess drug was introduced directly into the donor compartment, essentially identical diffusional curves were obtained. Maintaining sink receptor conditions in the present studies introduced complications. Because of the low aqueous solubility of the esters above butyl, the permeation could not be followed continuously spectrophotometrically as had been done previously. Two alternative methods were considered: (*a*) conversion of the free amine to the protonated species by desorbing in strong acid solution and (*b*) continuously flushing the receptor compartment with water to eliminate diffusant buildup. The former would have allowed continuous spectrophotometric assay but would have been nonspecific for a given compound. Impurities would have been read as the compound itself. Although the esters were believed to be in a high state of purity, this situation had to be avoided nonetheless. Therefore, a steady flushing of the receptor compartment was instituted followed by concentration and GC analysis. This procedure also tended to imitate biological absorption better by providing a simulated circulatory system to pick up the transported and desorbed compound.

A schematic representation of the total diffusional system is shown in Fig. 1. Obviously the components in the system are symbolically represented and are not drawn to scale. Basically the

system is composed of two independently circulating fluid phases separated within the diffusion cell by the membrane, F. The applied phase (donor phase) in which the drug exists in high concentration consists of the donor compartment, H, with about a 17-ml. capacity; a tubing pump, L; a thermostated reservoir, M, of 300-ml. capacity; and the interconnecting latex tubing. The reservoir contained excess drug which was excluded from the rest of the system by a screen affixed to the end of the siphoning tube, I. The reservoir was vigorously stirred with a magnetic stirring device, K. Stirring velocity in the diffusion cell compartments (stirrers not represented) was at 60 r.p.m. Constant temperature was maintained by circulating 37° water through the jacket of the reservoir and then to the bath into which the cell was immersed, N. Prior to initiating a run, the reservoir contents were pumped continuously through the tubing to saturate it with respect to the permeant.

The receptor system began with a large water reservoir, B, immersed in a larger constant-temperature bath (not shown) and stirred, A, to maintain 37°. Water was drawn from this source into and through the receptor compartment, G, by a piston pump, C, set to deliver exactly 20 ml./min. The flow continued to a spectrophotometer, D, through its flow cell (not shown) and to collecting vessels, E. Periodically during a run, the water reservoir, B, had to be replenished. This was always done with water heated to within a degree of 37°. Exact temperature equilibration was quickly established. The temperature drop from the reservoir to the collection vessel was found to be less than 0.5°. Fractions were collected on a 15-min. schedule for the short-chain esters (less than four carbon chain) and at 30- or 60-min. intervals for the higher homologs. Thus, the fractions ranged from 300 to 1200 ml.

Each fraction was extracted with three 75-ml. portions of chloroform. The chloroform extracts were brought to dryness on a Buchi vacuum evaporator. These were then set aside for GC determination.

In certain selected cases (*i.e.*, the determination of the true diffusivities of the methyl and ethyl esters using pure dimethylpolysiloxane films, the determination of the value of π by the permeability coefficient ratio, and the determination of the saturation-limited flux of the two lowest homologs), a previous procedure (12, 13) was employed. This was legitimate for the short esters because concentration buildup on the receptor side was insignificant at the termination of a run.

THEORETICAL

Steady-State Phenomena—Accurate interpretation of a membrane permeation experiment must be based upon sure knowledge of the source of the chemical potential gradient within the total barrier. For gaseous permeation of a membrane, from a region of high pressure or partial pressure to one of relatively low pressure, the gradient is almost entirely within the membrane because pressure equilibration is essentially instantaneous within the gaseous phases. This is not necessarily the case for permeation involving passage from a liquid phase into and through the membrane to a second liquid phase of lesser concentration. Fluid dynamics require the generation of relatively unstirred solvent layers adjacent to the stationary membrane surfaces due to viscous drag of the solvent against the membrane. These relatively stagnant regions are known as Nernst layers or diffusion layers and, in the permeation of a membrane, these layers must be treated as part of the total barrier. Taking note of this factor, Zwolinski *et al.* (17) included the diffusion layer and also the solvent-membrane interface in their treatment of biological membrane diffusion, a treatment in which they used the absolute reaction rate theory to describe the process. For thick membranes, interfacial contributions to barrier resistance may be neglected (13). Diffusion layers, on the other hand, must be accounted for in any general model.

Permeability equations for the diffusion layer–membrane system are derived assuming independent and additive resistances of the individual layers, *i.e.*:

$$R_T \text{ (total resistance)} = R_{AQ}{}^{d} + \frac{R_M}{(PC)} + R_{AQ}{}^{r} \qquad \text{(Eq. 2)}$$

where $R_{AQ}{}^{d}$ and $R_{AQ}{}^{r}$ are the respective resistances in the aqueous regions on the donor and receptor sides of the membrane, and R_M is the membrane resistance. An individual resistance is equal to the laminal thickness, h, divided by the diffusion coefficient of the permeant in that region, D, and thus:

$$R_T = \frac{h_{AQ}{}^{d}}{D_{AQ}} + \frac{h_M}{(PC)D_M} + \frac{h_{AQ}{}^{r}}{D_{AQ}} \qquad \text{(Eq. 3)}$$

The partition coefficient, (PC), is required to correct the concentration at the interfaces for differences in solvent and membrane affinities for the diffusant. A general equation for a number of like membranes placed in series is:

$$R_T = \frac{\Sigma h_{AQ}}{D_{AQ}} + \frac{\Sigma h_M}{(PC)D_M} = R_{AQ} + \frac{R_M}{(PC)} \qquad \text{(Eq. 4)}$$

This equation is derived assuming the solvent to be the same in all liquid compartments; comparable equations can be written for the more general case of unlike solvents and/or unlike membranes. The permeability of the total barrier, P, is the reciprocal of the total resistance and is, for a single membrane, sandwiched between two diffusion layers of identical thickness:

$$P = \frac{1}{R_T} = \frac{(PC)D_M D_{AQ}}{h_M D_{AQ} + 2h_{AQ}(PC)D_M} \qquad \text{(Eq. 5)}$$

Once penetration of the barrier has been effected, instantaneous flux through the total barrier can be expressed as $P(C^{d} - C^{r})$. For the boundary conditions of a receptor sink and constant donor phase concentration, C, the flux attains a steady state. This steady-state flux, F, is expressed by:

$$F = \left[\frac{(PC)D_M D_{AQ}}{h_M D_{AQ} + 2h_{AQ}(PC)D_M}\right] C \qquad \text{(Eq. 6)}$$

Equation 6 simplifies when $h_M D_{AQ} \gg 2h_{AQ}(PC)D_M$ to the familiar membrane control equation:

$$F = \left[\frac{D_M(PC)}{h_M}\right] C \qquad \text{(Eq. 7)}$$

Equation 6 also reduces to:

$$F = \left[\frac{D_{AQ}}{2h_{AQ}}\right] C \qquad \text{(Eq. 8)}$$

when $2h_{AQ}(PC)D_M \gg h_M D_{AQ}$. This situation represents a transfer from membrane to diffusion layer control of flux. In other words, the location of the concentration or, more precisely, activity gradient shifts from the membrane to the diffusion layers. It can be seen that in a system of fixed dimensions and invariant diffusivities, diffusion layer control is approached as the partition coefficient is increased. This may be expected to occur as one ascends a homologous series, since the partition coefficient grows exponentially with chain length while all other factors remain relatively constant. Equation 8 also predicts that the steady-state flux is independent of membrane thickness or any other membrane property under diffusion layer control.

Equations 7 and 8 indicate that the steady-state flux is directly proportional to concentration in the donor phase regardless of the flux-determining mechanism (assuming sink receptor conditions). Since, in any normal situation, the concentration in the applied phase has as its limiting value the solubility of the compound, the limiting value of the steady-state flux is determined by the donor phase solubility of the diffusant. Therefore, the maximum flux in a given membrane system can be accurately estimated knowing D_{AQ}, D_M, (PC), Σh_M, Σh_{AQ}, and the donor solubility of the permeant, S. The appropriate expression, with some rearranging of terms, is:

$$\lim_{C \to S} F = F^{s} = \left[\frac{(PC)}{\frac{2(PC)h_{AQ}}{D_{AQ}} + \frac{h_M}{D_M}}\right] S \qquad \text{(Eq. 9)}$$

which can also be expressed in a convenient logarithmic form:

$$\log [F^{s}] = \log S + \log (PC) - \log \left[\frac{2(PC)h_{AQ}}{D_{AQ}} + \frac{h_M}{D_M}\right] \qquad \text{(Eq. 10)}$$

To develop a general expression for the maximum flux of each

member of a homologous series, it is necessary to relate each of the aforementioned parameters to the chain length of the homolog under consideration. For a given system the membrane thickness can usually be held constant and the diffusion layers fixed by controlling the cell geometry, stirring rate, *etc.* It is expected that the increasing molecular size (volume) of the congeners as the series is ascended will result in decreases in both the aqueous diffusivity, D_{AQ}, and the membrane diffusivity, D_M. However, these decreases would be slight for a methylene unit added to a molecule already of appreciable size. Moreover, examination of Eq. 9 indicates that the effect will not influence relative membrane or diffusion layer control since both D_{AQ} and D_M would be decreasing simultaneously, likely at about the same rate. Therefore, in the following derivations the respective diffusivities are assumed to be invariant within the series.

Partition coefficients for members of a homologous series between immiscible polar and nonpolar phases invariably increase by a constant factor as the series is ascended (23). Thus, the relationship between the partition coefficient and alkyl chain length may be conveniently expressed for the nth compound in a series by:

$$\log (PC)_n = \log (PC)_0 + \pi n \qquad \text{(Eq. 11)}$$

where $(PC)_0$ is the partition coefficient of a hypothetical reference congener in the series containing no methylene units. This makes it the Y intercept of a plot of log (PC) against n. The value, π, is the log of the increase per methylene unit and is essentially constant through a reasonably lengthened series. It is, however, dependent on the natures of the two immiscible phases (24) and tends to increase as the polarity difference between the two phases increases. The symbol, n, represents the number of carbons in the chain.

According to the work of Saracco and Marchetti (25), the aqueous solubilities of organic homologs, liquid or crystalline, decrease regularly with increasing chain length in much the same fashion as the partition coefficient grows. This is somewhat surprising because definite, odd–even alteration in solubility in other reasonably polar solvents is generally observed for crystalline materials. The regularity of the incremental decreases affords expression of any given congener's aqueous solubility by:

$$\log S_n = \log S_0 - \delta n \qquad \text{(Eq. 12)}$$

where S_n is the solubility of the nth congener in the series, S_0 is the solubility of the hypothetical zero chain length homolog, and δ is the log of the factor by which the solubility decreases between any two adjacent homologs. The value, δ, is thus arbitrarily defined as a positive quantity, and the decreasing solubility is accounted for by the negative sign.

In cases where the logarithm of solubility is linearly related to chain length, an expression can be derived from Eqs. 10–12 relating the maximum steady-state flux for the nth homolog of a series to its chain length and the physicochemical properties of the reference homolog:

$$\log F_n^s = \log S_0 + \log (PC)_0 + (\pi - \delta)n - \log [R_{AQ}(PC)_0 10^{\pi n} + R_M] \qquad \text{(Eq. 13)}$$

In this equation, F_n^s is the saturation-limited flux of the nth homolog, and R_{AQ} and R_M are the total aqueous and membrane resistances, respectively, as previously defined (Eq. 4). For long-chain homologs (large values of n), $R_{AQ}(PC)_0 10^{\pi n} \gg R_M$ and Eq. 13 reduces to:

$$\lim_{n \to \infty} \log F_n^s = \log S_0 - \log R_{AQ} - \delta n \qquad \text{(Eq. 14)}$$

This indicates that the maximum possible flux is linearly related to n in the same manner as log S. If Eq. 12 is subtracted from Eq. 14, it is found that the concentration-normalized flux for large values of n (large partition coefficients) is a constant equal to $1/R_{AQ}$ or the solvent diffusivity divided by the sum of the solvent diffusion layer thicknesses. If D_{AQ} is known or can be determined independently, this provides a means of estimating Σh_{AQ}.

For small values of n, it is possible that $R_M \gg R_{AQ}(PC)_0 10^{\pi n}$ and:

$$\log F_n^s = \log S_0 + \log (PC)_0 + (\pi - \delta)n - \log R_M \qquad \text{(Eq. 15)}$$

Since three of the four terms in Eq. 15 are constants, the magnitude and sign of the steady-state flux change in the region where this equation is valid depend solely on the relative magnitudes of π and δ. If $\pi > \delta$, there is a maximum or point of optimized flux at some positive value of n, the overall profile appearing "parabolic[7]." In this interesting situation, the chain length yielding the optimized or maximum flux may be found by differentiating Eq. 13 with respect to n and setting the derivative equal to zero:

$$\frac{d[\log F_n^s]}{dn} = \pi - \delta - \frac{R_{AQ}(PC)_0 10^{\pi n} \pi}{R_{AQ}(PC)_0 10^{\pi n} + R_M} = 0 \qquad \text{(Eq. 16)}$$

The optimized value of n obtained is:

$$n_{\text{optimum}} = \frac{1}{\pi}\left(\log\left[\frac{\pi - \delta}{\delta}\right] + \log\left[\frac{R_M}{R_{AQ}}\right] - \log(PC)_0\right) \qquad \text{(Eq. 17)}$$

As can be seen from Eqs. 16 and 17, if $\pi < \delta$, there is no point of optimization, the largest steady-state flux being seen for the hypothetical zero chain length homolog. Regardless of the relative magnitudes of π and δ, if the solubility expression is subtracted from Eq. 15, a new expression results:

$$\log F_n^{c-1} = \log \frac{(PC)_0}{R_M} + \pi n \qquad \text{(Eq. 18)}$$

Thus, the value of π can be obtained from the limiting slope as $n \to 0$ of a plot of F_n^{c-1} *versus* R. The term F_n^{c-1} is the concentration-normalized flux. Normalization to any arbitrary concentration is possible without affecting the value of π.

The concepts and mathematical treatment advanced here are not necessarily predicated on the logarithm of either the partition coefficient or the solubility function being directly related to n. If each physicochemical property can be mathematically approximated and the resulting equation differentiated, comparable expressions to those already presented can be derived. In the specific case presented in this report, solubilities of *p*-aminobenzoates were found to be nonuniformly continuous with a break at the butyl ester (Fig. 5). Since a second-order equation gave a reasonable fit to the solubility profile, this equation was used in the computer analysis. Details are presented in the *Discussion* section.

Nonstationary State—Characterization of the nonstationary state is of equal importance, from both theoretical and practical standpoints, to an understanding of steady-state processes. Phenomena associated with membrane control of flux are reasonably well understood. The basic equation applicable to homogeneous membranes was originally derived by Daynes (26) and later generalized by Barrer (27):

$$t_L = \frac{h_M^2}{6D_M} \qquad \text{(Eq. 19)}$$

This equation states that the lag time is dependent only on membrane thickness and membrane diffusivity. Permutations on this equation treating the complexities of inhomogeneity within the barrier also were published (12, 28, 29). However, until recently, factors determining the lag time in diffusion layer control of flux were unchartered. Flynn *et al.* (30) showed that the cumulative amount, M, of material through the barrier per unit area at any time, t, for the diffusion layer control situation may be expressed by:

$$M = \frac{D_{AQ}C}{2h_{AQ}}\left\{t - \frac{(PC)h_M h_{AQ}}{2D_{AQ}}\left(1 - e^{-2D_{AQ}t/(PC)h_M h_{AQ}}\right)\right\} \qquad \text{(Eq. 20)}$$

when the diffusion layers are of equivalent thickness and like solvent is used for both donor and receptor phases.

As t increases, M becomes a linear function:

$$\lim_{t \to \infty} M = \frac{D_{AQ}C}{2h_{AQ}}\left\{t - \frac{(PC)h_M h_{AQ}}{2D_{AQ}}\right\} \qquad \text{(Eq. 21)}$$

[7] The strict mathematical requirements for a parabola would not be satisfied, the equation actually being nearer to a skewed hyperbola.

Table III—Summary of 37° Diffusional Data Using 476-μm. Membranes

p-Aminobenzoate Ester	Run	Lag Time, min.	Steady-State Flux, Saturated Solutions, mg./hr.	Average Steady-State Flux, Saturated Solutions, mmoles/hr.	Concentration Normalized Steady-State Flux[a] × 10^3, $hr.^{-1}$
Methyl	1	19.5	0.371	2.46×10^{-3}	0.0972
Ethyl	1	22.5 (22.5)[b]	1.03 (1.03)[b]	6.24×10^{-3}	0.612
	2	22.5	1.03		
Propyl	1	21 (20)[b]	1.27 (1.40)[b]		
	2	18	1.38	7.82×10^{-3}	1.66
	3	21	1.56		
Butyl	1	15 (16.5)[b]	1.23 (1.40)[b]	7.25×10^{-3}	4.22
	2	18	1.57		
Pentyl	1	44 (41.5)[b]	0.657 (0.653)[b]	3.15×10^{-3}	8.08
	2	39	0.648		
Hexyl	1	69 (71)[b]	0.217 (0.242)[b]		
	2	61	0.298	1.10×10^{-3}	10.6
	3	82	0.212		
Heptyl	1	120 (125)[b]	0.060 (0.062)[b]		
	2	120	0.055	0.26×10^{-3}	13.0
	3	135	0.071		

[a] Average steady-state flux (previous column) divided by the respective solubility in mmoles. [b] Average of set.

which has the steady-state flux, $D_{AQ}C/2h_{AQ}$, as its slope. This steady-state expression is identical to Eq. 8, which also was derived assuming equivalently thick diffusion layers on each side of the membrane. The lag time in diffusion layer flux control is obtained by setting $M = 0$ or its equivalent, plotting and extrapolating the steady-state portion of the curve to the time axis. Based on Eq. 21, it is:

$$t_L = \frac{(PC)h_M h_{AQ}}{2D_{AQ}} \qquad \text{(Eq. 22)}$$

However, Eq. 22 is for the special circumstance that $h_{AQ}{}^d = h_{AQ}{}^r$. This is not the situation in the present studies due to placement of the membrane support screen in the system. The general literature expression for lag time reduces to (30):

$$t_L = \frac{(PC)h_M h_{AQ}{}^d h_{AQ}{}^r}{D_{AQ}(h_{AQ}{}^d + h_{AQ}{}^r)} \qquad \text{(Eq. 23)}$$

Considering the relationship of (PC) to chain length, it is expected that the lag time will increase exponentially upon ascending a homologous series once diffusion layer control of permeation is attained. Moreover, both total diffusion layer thickness and membrane thickness must be accounted for as must the aqueous diffusivity. Equations 20–23 may be written in terms of diffusion layer resistance as defined in Eqs. 2–4. Equation 23 becomes:

$$t_L = (PC)h_M \Big/ \left(\frac{1}{R_{AQ}{}^d} + \frac{1}{R_{AQ}{}^r}\right) \qquad \text{(Eq. 24)}$$

Thus, as might have been expected, the resistance encountered in the diffusion layers determines the lag time and, indeed, the steady-state flux (Eq. 21). The thickness of the membrane and the partition coefficient are involved since they determine the capacity of the membrane for the diffusant and the membrane acts as a reservoir for the diffusant in diffusion layer control. To our knowledge, these equations have never been experimentally validated.

RESULTS

Membrane Permeation Studies—Representative diffusional curves for the permeation of several odd chain length *p*-aminobenzoates from saturated solutions through 476-μm. membranes at 37° are shown in Fig. 2. These data are presented as cumulative milligrams penetrated as a function of time. Each curve is characteristic for a given ester in limiting slope of the steady-state line and its extrapolated lag time or point of intersection with the time axis. The curves indicate that:

1. There is initially an increase in flux in the steady state as the homologous series is ascended.

2. The flux drops off markedly at longer chain lengths. Additionally, lag times, which appear to be approximately constant initially, increase sharply for the longest esters. Diffusional data obtained in this fashion for the uninterrupted ester series, methyl to heptyl, are summarized in Table III. These data indicate reasonable experimental reproducibility and illustrate the ester-specific slopes and intercepts, reinforcing the conclusions drawn from the odd chain length ester profiles.

When the logarithm of the steady-state flux from saturated solutions is plotted against n, the number of carbons in the ester chain, a "parabolic" curve is described (Fig. 3, filled circles). This plot crests between $n = 3$ and $n = 4$, with a marked acclivity and declivity as the homologous series is ascended. The estimated slope of a line drawn asymptotically to the left-hand portion of the curve is 0.189, which amounts to a 1.55-fold increase in flux per methylene unit. The right-hand asymptote is quite steep, each methylene unit leading to a 4.42-fold decrease in steady-state flux.

The averaged nonstationary-state behavior (averaged lag times) for the diffusional runs are plotted semilogarithmically against ester chain length in Fig. 4. The plot indicates that there might be a slight decrease in lag times up to $n = 4$, but this is uncertain within experimental error. For the pentyl ester and above, the lag times appear to increase exponentially. Previous studies with commercial dimethylpolysiloxane films demonstrated that the silica filler in the material markedly lengthened lag times due to adsorption of the

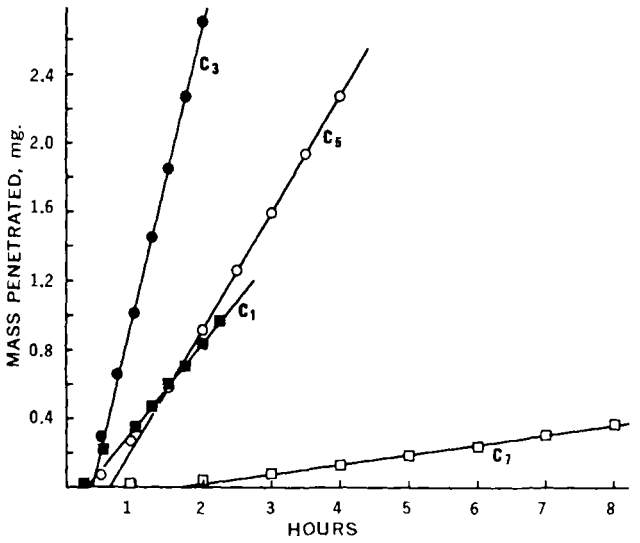

Figure 2—*Cumulative milligrams penetrated through 0.0476-cm. membranes for the odd chain length esters studied at 37° as a function of time. C_1, C_3, C_5, and C_7 designate the methyl, propyl, pentyl, and heptyl derivatives, respectively.*

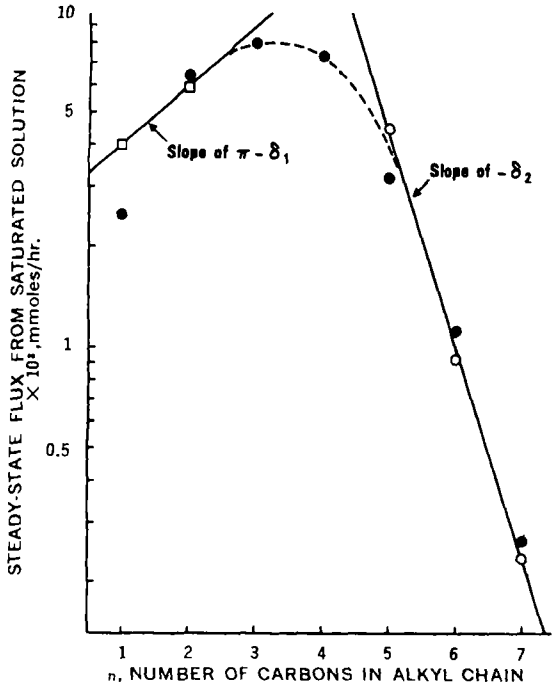

Figure 3—*Steady-state flux from saturated solution plotted against the ester chain length. The circles are data obtained with the GC procedure. Key: ●, runs using 0.0476-cm. membranes; ○, runs using 0.0126-cm. membranes; and □, data points for spectrophotometric runs using 0.0476-cm. membranes. Slopes of* $\pi - \delta_1$ *(0.189) and* $-\delta_2$ *(−0.625) were fitted to the data with good results.*

diffusant, the lag time ratio to pure dimethylpolysiloxane membranes of comparable thickness being about seven for ethyl *p*-aminobenzoate (12). The plateau or near plateau from $n = 1$ up to $n = 4$ in Fig. 4 suggests that adsorption for the methyl, ethyl, propyl, and butyl esters is similar qualitatively if not quantitatively. The increases beyond butyl might be attributed to a change in adsorption mechanism, but this degree of change would be extremely unlikely and a more compatible explanation of the phenomenon needs to be formulated. As detailed later, the observed behavior is consistent with a change from membrane to diffusion layer flux control.

If diffusion layers are the principal determinant of the steady-state flux for the pentyl and higher esters, then the flux should be independent of membrane properties in this region. For this reason the effect of reducing membrane thickness from 476 to 126 μm. on the permeation rate of the pentanoate, hexanoate, and heptanoate was assessed. Conditions were otherwise exactly the same as used previously. The slopes and lag times for these runs are summarized in Table IV. Additionally, the steady-state data are plotted in Fig. 3 (open circles). The observed flux values were essentially the same as were observed for the thicker membranes, particularly when experimental error is considered. Lag times, on the other hand, were significantly abbreviated.

Much of the interpretation of these data is predicated on constant diffusivity throughout the homologous series. While the lag times and the apparent diffusivities calculated therefrom covering the first four members of the series suggest that the diffusivity is reasonably constant, the possibility exists that this is misleading due to offsetting adsorption and diffusivity changes. Therefore, the dif-

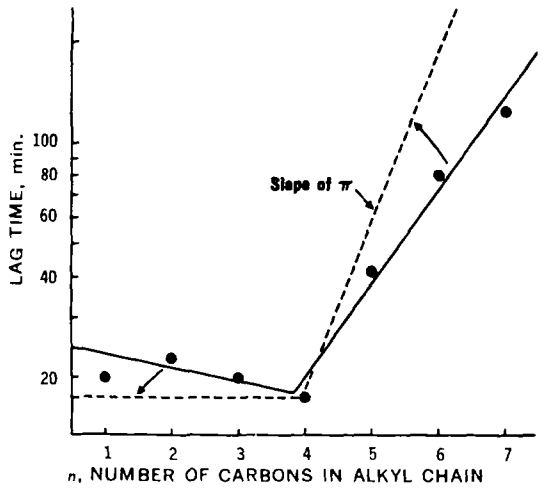

Figure 4—*Plot of the lag time against ester chain length for the alkyl* p*-aminobenzoates. Conditions were 37°, saturated solutions, and 0.0476-cm. membranes. The dotted curve represents a shift in the profile, which would be expected if adsorption on silica filler in the membrane were decreasing uniformly through the series. A slope of* π *(0.540) is theoretically predicted in the region of diffusion layer control (~butyl to heptyl).*

Table IV—Summary of 37° Diffusional Data Using 126-μm. Membranes

	p-Aminobenzoate		
	Pentyl	Hexyl	Heptyl
Steady-state flux, saturated solutions, mg./hr.	0.930	0.201	0.055
Steady-state flux, saturated solutions, mmoles/hr.	4.49×10^{-3}	0.91×10^{-3}	0.23×10^{-3}
Concentration-normalized flux[a] × 10^3, $hr.^{-1}$	11.5	8.75	11.5
Lag time, 126-μm. membrane	6.5 min.	18 min.	33 min.
Lag time, 476-μm. membrane	42 min.	71 min.	125 min.
Lag time extrapolated to 476-μm. membrane from 126-μm. data, diffusion layer control	26 min.	69 min.	126 min.
Lag time extrapolated to 476-μm. membrane from 126-μm. data, membrane control	93 min.	258 min.	470 min.

[a] Steady-state flux divided by concentration in nmoles.

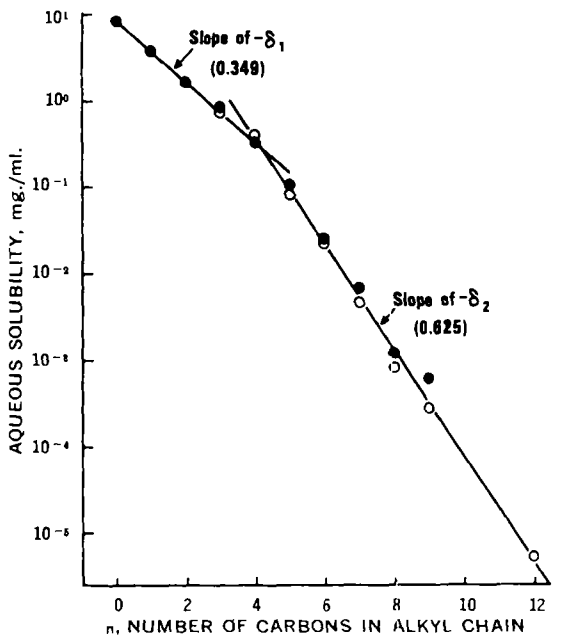

Figure 5—*Solubility of the alkyl* p*-aminobenzoates in water at 37°. Key: ●, data obtained spectrophotometrically; and ○, data obtained by GC. There is a distinct break in the curve at butyl, the slopes on each side of this point being −0.349 and −0.625, respectively.*

Table V--Solubilities of the Alkyl *p*-Aminobenzoates in Water at 37°

Compound	Solubility, mg./ml., by UV Analysis	Solubility, mg./ml., by GC Analysis	Molecular Weight	Millimolar Solubility, Best Method[a]	Solubility Approximation, Second-Order Equation
p-Aminobenzoic acid	8.28 (3)[b]	—	137	60.4	76.4
Methyl *p*-aminobenzoate	3.82 (2)[b]	—	151	25.3	28.9
Ethyl *p*-aminobenzoate	1.68 (3)[b]	—	165	10.2	10.3
Propyl *p*-aminobenzoate	0.841 (4)[b]	—	179	4.70	3.45
Butyl *p*-aminobenzoate	0.331 (3)[b]	—	193	1.72	1.08
Pentyl *p*-aminobenzoate	0.106 (4)[b]	0.081	207	3.9×10^{-1}	3.2×10^{-1}
Hexyl *p*-aminobenzoate	0.024 (3)[b]	0.023	221	1.04×10^{-1}	8.9×10^{-2}
Heptyl *p*-aminobenzoate	0.0068 (3)[b]	0.0046	235	2.0×10^{-2}	2.3×10^{-2}
Octyl *p*-aminobenzoate	0.0012 (2)[b]	0.00079 (2)[b]	249	3.2×10^{-3}	5.7×10^{-3}
Nonyl *p*-aminobenzoate	0.0006 (3)[b]	0.00027 (3)[b]	263	1.02×10^{-3}	1.3×10^{-3}
Dodecyl *p*-aminobenzoate	—	≃0.000005	305	$\simeq 1.6 \times 10^{-5}$	1.1×10^{-5}

[a] UV up to pentyl, GC pentyl through dodecyl. [b] Number of determinations if more than one.

fusivities of the methyl and ethyl esters were measured using fillerless dimethylpolysiloxane membranes. These esters were chosen because of their greater aqueous solubilities, making it possible to maintain sink conditions in continuous spectrophotometric measurement, and because a molecular weight effect would be more pronounced at the lower end of the series. The calculated diffusivity for methyl *p*-aminobenzoate and for ethyl *p*-aminobenzoate was found to be 2.71×10^{-6} and 2.72×10^{-6} cm.²/sec., respectively, each being measured at 37° using 559-μm. membranes. The latter is in excellent agreement with the value of 2.67×10^{-6} cm.²/sec. estimated previously (12).

Solubility Measurements--To coordinate and interpret the diffusional data from saturated solutions, the solubility of each ester at 37° in water, the donor phase solvent, was sought. Two analytical methods were used, spectrophotometry and GC. The spectrophotometric method was convenient and fast and likely provided reasonable data for the shorter, more soluble compounds since all were carefully prepared and purified. For long-chain esters, the GC technique was preferred, because it provided for simultaneous separation and quantitation. Thus, it minimized error due to the presence of trace, but spectrophotometrically significant, impurities. The solubilities by both methods are summarized in Table V in both milligrams per milliliter and moles per liter. It can be seen that the UV and GC assays gave comparable results where they overlapped. The GC values are generally smaller, consistent with the nonspecific nature of the UV procedure. These data are plotted as the logarithm of solubility *versus* chain length in Fig. 5. It is evident that the solubility dependency has two distinctly different regions, with the change in behavior occurring at the butyl ester[8]. The solubility of benzoic acid was also determined and, interestingly, it is aligned with the trend evident for the shorter esters. The slope of the line through this region based on graphical interpolation is 0.349; thus, each methylene unit decreases the solubility by a factor of 2.24. Similarly, for the esters past the butanoate, there is a slope of 0.645, amounting to a 4.42 decrease per methylene addition. Solubilities were obtained to the dodecanoate. At this point the solubility was only slightly greater than the threshold of detection by the GC procedure. Attempts to measure the solubility of the hexadecanoate were obviously unsuccessful. Based on the extrapolated slope for the longer esters, its solubility would be in the vicinity of 1×10^{-8} mg./ml. It will be shown in a future report that the break in the solubility curve is attributable to a change in the basic crystal structure of the compounds (31). Support of this conclusion (aside from the aqueous solubility curve) was drawn from X-ray diffraction, organic solubility, and melting-point profiles.

DISCUSSION

Aqueous Solubility of Organic Homologs--Since the solubility of a nonelectrolyte is the determinant of many phenomena of pharmaceutical interest, relationships generalizing and organizing solubility are potentially of great utility. Solubilities of organic homologs in organic solvents lack predictability as an uninterrupted series since odd-even alterations are observed as the series is ascended. In this regard, aqueous solubilities appear to be unique because these odd-even alterations are not generally observed (25). Of equal importance is the observation that aqueous solubilities decrease by a constant decrement as chain length is increased, with the result that a plot of the logarithm of the solubility against chain length is linear (25). These factors, taken together, indicate that the aqueous solubilities of an entire homologous series may be estimated by determining the solubilities of just a few homologs. Furthermore, since the log of the decremental decrease (designated in this paper as the delta value, δ) is confined within fairly narrow limits, *i.e.*, from about 0.5 to about 0.7, it is possible to estimate reasonably the solubility of an adjacent homolog without knowledge of the exact relationships by assuming a value for δ of 0.6.

Published solubilities of homologous series were carefully organized and analyzed by Saracco and Marchetti (25). They expressed solubility in equivalent form to that in Eq. 12; but since they formulated their equation in natural logarithms, their reported constants are 2.303 times larger than the δ values defined in this paper. Of the approximately 20 series processed, only one, the straight-chain fatty acids, exhibited a change in slope. The change was to a lesser slope and occurred at nonyl. This behavior was later shown to be attributable to unsuppressed ionization at the longer chain lengths (32).

It can be seen in Fig. 5 that the logarithm of the solubilities of the alkyl *p*-aminobenzoates are linearly related to chain length but that there is also a change in dependency for this series at butyl. The δ_1 and δ_2 values for each portion of the curve are 0.349 and 0.625, respectively. The former is less than any of the values previously reported; the latter is reasonably typical. Unlike the fatty acids, this change cannot be accounted for by unsuppressed ionization because the change is to a greater and not lesser declivity. Furthermore, based upon the pH of the saturated solutions and the known pKa, the contributions of the ionized species can be shown to be negligible. When the solubility trend is compared with melting-point behavior and other physical evidence [reported separately (31)], a clear indication of a basic change in molecular order (unit cell) within the crystals emerges. Thus, from the standpoint of crystal structure and the solubility dependent thereon, the "molecular tail eventually becomes sufficiently large to wag the molecular dog."

Because the ultimate purpose of obtaining the solubility data was to coordinate membrane transport with equations expressing transport as a function of solubility, the nonuniformly continuous nature of the solubility was troublesome. It forced exact mathematical characterization into two stages and complicated differentiation. Therefore, the solubilities were fitted to a second-order equation:

$$\log S_n = \log S_0 - \delta n - \epsilon n^2 \qquad \text{(Eq. 25)}$$

The values of δ and ϵ were computer fitted to the experimental data in Table V (from *p*-aminobenzoic acid to the dodecyl ester) and are 0.408 and 0.0134, respectively. The approximated solubilities using

[8] Although there is a break in the solubility curve coinciding with the break in the flux profile (Fig. 3), partitioning is not similarly affected. The logarithm of the partition coefficient between silicone oil and water was found to be linear with chain length from methyl to dodecyl instead (31).

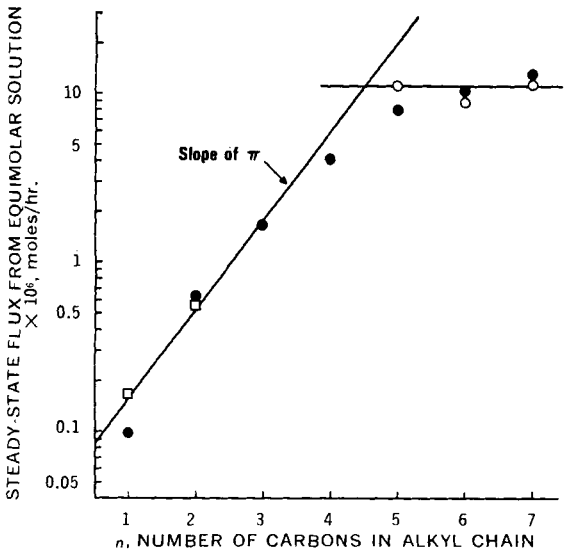

Figure 6—*Plot of concentration-normalized flux* versus *alkyl chain length. Key:* ○, *GC runs using 0.0126-cm. membrane;* ●, *GC runs using 0.0476-cm. membranes; and* □, *spectrophotometric runs. The independently obtained slope of* π *(0.540) is fitted to the data for the short esters (membrane control) with good results.*

this function are included in Table V for comparison with the actual data. It can be seen that the second-order function gave quite reasonable estimations throughout the range.

Steady-State Permeation of Model Membrane by the Alkyl *p*-Aminobenzoates—The principles governing diffusion of solutes through liquid or semisolid phases have extremely broad application in pharmacy and related disciplines because they determine dissolution and membrane permeation rates, absorption and biodistribution of drugs, and, in some instances, chemical reactivity, *etc.* Numerous *in vivo* and *in vitro* studies have encompassed the varied aspects of membrane transport. However, these have been made with such a diverse array of membranes (human skin to cellophane), conditions, and permeants that they preclude collation except in the most general of terms. Any valid thrust into the problem must be based on careful analysis of the variables that would be encountered. Only by varying one parameter at a time can conclusions be drawn as to the effect of that parameter on the system. Of particular importance is the influence of the physicochemical properties of the diffusant on the permeation process. Because of the additive-constitutive nature of certain molecular properties, it is possible to introduce definite, decremental changes in diffusant property over a wide range by increasing chain length one methylene unit at a time. This was the format for the present study.

The selection of dimethylpolysiloxane as the prototype membrane was based on its uniquely high permeability and its lack of affinity for polar solvents, especially water. These properties enabled diffusional studies uncomplicated by imbibed solvent and a commensurate loss in membrane integrity to be performed. Since dimethylpolysiloxane is a continuous, nonporous, and nonpolar membrane, a partitioning step is required in the permeation process. This is a major point of dissimilarity relative to some cellulosic films, which absorb water to an extent that the dry weight is only a small fraction of the total hydrated weight. Consequently, the solubility of the diffusant in the highly hydrated barrier is essentially the solubility in the aqueous regions; thus the partition coefficient is not much different from unity regardless of the diffusant selected. Additionally, unless the hydration is instantaneous, there is a time dependency in the barrier property of the cellulosic membrane not observed in the dimethylpolysiloxane case.

Alkyl *p*-aminobenzoates were selected as the model diffusants because of their known permeability through dimethylpolysiloxane (11, 12) and their ease of preparation. Saturated solutions of these esters were used as a means of maintaining a constant donor concentration and to provide maximal diffusion rates. The steady-state flux profile from saturated solutions (Fig. 3) indicates a maximum located somewhere between the ethyl and butyl esters. Since there is also a break in the solubility relationship in this region, the change in solubility is suspect as the shape-determining factor. However, a more thorough examination indicates that the magnitude of the change far exceeds that which could be expected from the solubility trend alone.

The data are consistent with a change from membrane to diffusion layer control of flux. In other words, the gradient, which is essentially entirely within the membrane for the short esters, gradually shifts to the diffusion layers as chain length or the partition coefficient is increased (Eqs. 7 and 8). The concentration drop across the membrane eventually decreases to a point of insignificance. Interpretive mathematical expressions for diffusion layer control are presented in the *Theoretical* section. According to Eq. 15, the limiting upward slope for the short esters is equal to $\pi - \delta_1$. According to Eq. 14, the limiting slope on the other side of the maximum should be equal to $-\delta_2$. The value of π was determined by several independent methods, specifically from the ratio of methyl and ethyl *p*-aminobenzoate partition coefficients determined kinetically with pure silastic membranes (0.560), from the ratio of steady-state permeabilities of these two esters at equimolar concentration through filled membranes (0.509, 0.530, and 0.518), from partitioning of these and some closely related compounds between silicone oil and water (0.540), and from the ratio of published permeabilities (7) of several homologous *p*-aminoacetophenones (0.540). Assuming a value of 0.540 to be representative, $\pi - \delta_1$ is equal to 0.189. The limiting slopes drawn to the flux curve (Fig. 3) are equal to $\pi - \delta_1$ or 0.189 and δ_2 or 0.625. The agreement for diffusion layer control is excellent (right-hand slope). The agreement on the left-hand side is also good, particularly the fit to the spectrophotometric data[9].

If the steady-state flux from saturated solutions (in units of millimoles per hour) for each ester is divided by that ester's solubility (in millimoles per liter), the steady-state flux for a solution of unit molarity is obtained. This concentration normalization produces theoretical values because the compounds are not this soluble. Regardless, the comparison at equimolar concentration is important since it demonstrates some of the phenomenological trends and provides a means of calculating the value of π and the total diffusion layer thickness. Figure 6 is a plot of the logarithm of the concentration-normalized flux for the alkyl *p*-aminobenzoates for both 0.0476- and 0.0126-cm. thickness membranes against their ester chain length. The ascending portion of the curve is fitted with a line of slope equal to 0.540, the independently determined π value. It can be seen to be in very acceptable agreement with the data. The slope of π in the membrane control region in this plot is predicted by Eq. 18. At about butyl the curve begins to level and is essentially flat at hexyl. This is in agreement with the predictions of Stehle and Higuchi (1), who first recognized this to be a consequence of the attainment of diffusion layer control. Their theoretical plot differs only in that they used the log of the partition coefficient in lieu of *n*. When Eq. 12 is subtracted from Eq. 14, the plateau region is described mathematically.

Since the value of the steady-state flux at the plateau is equal to $D_{AQ}/\Sigma h_{AQ} \times C$, and since C has been normalized to a fixed concentration, the total thickness of the diffusion layers is calculable, providing the aqueous diffusivity and membrane cross-sectional area are known. For these compounds, D_{AQ} is about 6×10^{-6} cm.²/sec. And since C is 1 mmole/l. or 1×10^{-3} mmole/cm.³, the diffusion layer thickness is about 0.0188 cm. This thickness would be surprising considering the stirring rate and the proximity of the stirrer to the membrane were it not for the membrane support screen. This has the effect of retarding mixing on its side of the barrier at the membrane surface, with a subsequent increase in the effective diffusion layer thickness.

To determine some of the fundamental diffusional constants, the permeation of pure, fillerless dimethylpolysiloxane membranes by methyl and ethyl *p*-aminobenzoates was studied. By using the lag time method (26, 27), the respective diffusivities are 2.71×10^{-6} and 2.72×10^{-6} cm.²/sec. The ratio of the permeability to the diffusivity gave partition coefficients of 0.0896 for the methyl ester and 0.326 for the ethyl ester. The latter is only about one-third that reported previously by Most (11). He determined his value spectrophotometrically by equilibration of pure dimethylpolysiloxane at 25°. This method as employed is less suitable for low

[9] The spectrophotometric data points are an average of three runs. The spectrophotometric and GC data were in acceptable agreement.

partition coefficients because it depends on the measurement of small spectral changes in relatively large numbers. The logarithm of the ratio of these partition coefficients gave one of the estimates of π: 0.560.

By using the value of π (average of all estimations about 0.540) and the partition coefficients obtained for the methyl and ethyl derivatives, it is possible to calculate the partition coefficients of the other series members. Of interest is the partition coefficient resulting in equal contributions to total resistance from the membrane and diffusion layers. To accomplish this, one merely has to let $h_M/(PC)D_M = \Sigma h_{AQ}/D_{AQ}$. By substituting in the appropriate values for the various parameters and 0.0476 cm. for h_M, a value of 5.58 is obtained. This corresponds to a carbon number of 3.46. Therefore, one can expect the propyl ester flux to be principally membrane controlled but the butyl ester flux to be appreciably displaced from the membrane control line, and this situation is observed.

Nonstationary-State Behavior—Lag times for the alkyl *p*-aminobenzoates are listed in Table III and plotted semilogarithmically against ester chain length in Fig. 4. According to the classical lag time expression (Eq. 19), which is only applicable to membrane control, the lag time at constant thickness should only reflect differences in diffusivities of different species. Since diffusivity is assumed to remain essentially constant within the homologous series (at least for the limited span of methyl to heptyl), the lag time should have been invariant. This is roughly the observed case up to the butyl ester. The lag time appears to grow exponentially thereafter. In processing the steady-state data, it was shown that diffusion layer control of flux was obtained past the butyl derivative. Equation 23 is a representation of the lag time dependency in this situation. The direct dependence on the membrane–water partition coefficient should lead to an exponential increase in lag time as chain length is increased once diffusion layer control is reached. Furthermore, the slope of the line should also be equal to π. As can be seen from Fig. 4 the expected features of the log (lag time) dependency are all qualitatively observed. However, the region of logarithmic increase has a slope (roughly 0.34) significantly less than π (0.540).

It has been shown that the lag time for the permeation of dimethylpolysiloxane membranes containing silica filler by ethyl *p*-aminobenzoate may be reasonably fitted to (12):

$$t_L = \frac{h_M^2}{6D_M}(1 + KV_2) \qquad \text{(Eq. 26)}$$

where V_2 is the filler volume fraction and K is an adsorptive constant. KV_2 was shown to be appreciably greater than 1 (12). It is expected that other alkyl *p*-aminobenzoates will show the same dependency qualitatively (membrane control only), but it is not expected that K will be constant throughout the series. Indeed, the high polarity of the silica surface relative to the dimethylpolysiloxane continuum makes a linear decrease in log K with increasing chain length predictable (33). A decrease in adsorption will affect the lag time in similar fashion in membrane control and diffusion layer control since K appears in the partition coefficient term of the latter. If such a relationship is assumed, then the line through the points for the long-chain esters in Fig. 4 can be pivoted counterclockwise about the butyl ester to merge with a line drawn with a slope of π. This can be done without significantly changing the dependency in the membrane control region considering experimental error. In effect, the apparent partition coefficient is not growing as fast as the true partition coefficient since the relative amount adsorbed is decreasing with increasing n. A similar analysis is not applicable to the increase in steady-state flux from concentration-normalized solutions, because the adsorptive processes are satisfied prior to attainment of the steady state and the increase in permeability (membrane control) is a true reflection of the increase in the partition coefficient between the membrane continuum and the aqueous phase.

Equation 23 indicates a direct linear dependency of lag time on membrane thickness. This was tested by comparing lag times for 0.0126-cm. membranes to those found at 0.0476 cm. These data are summarized in Table IV. Also included are calculated values for the lag time at 0.0476-cm. thickness based on membrane and diffusion layer control equations and the 0.0126-cm. thickness data. The data for the pentyl ester suggest that the permeation is intermediate between membrane and diffusion layer control. It is possible that the permeation of the pentyl ester through the thicker membrane is not totally in diffusion layer control. The hexyl and heptyl esters, which are clearly in diffusion layer control (Figs. 3 and 6), have the exact membrane thickness lag time dependency predicted for them. The membrane control predicted lag times for these two esters are enormously longer than those actually observed.

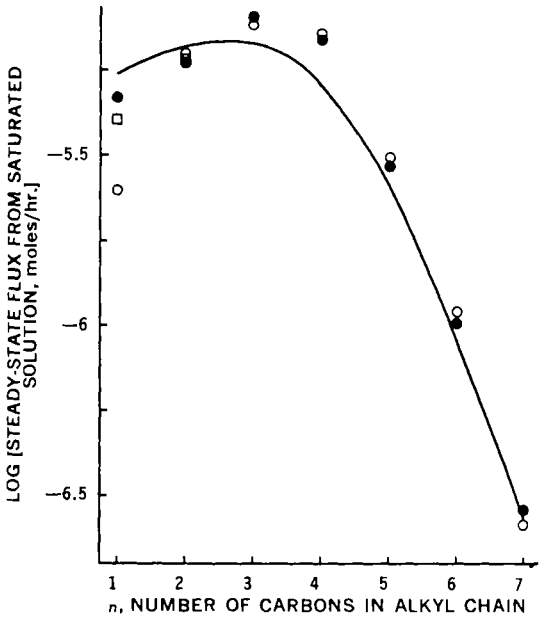

Figure 7—*Computer-drawn curve (——) for log [flux] against chain length, using the second-order solubility approximation. The open circles, ○, and squares, □, are the actual data found with 0.0476-cm. membranes gas chromatographically and spectrophotometrically. The filled circles, ●, are calculated points using the actual raw solubility data and estimated diffusional parameters (see text).*

Considering everything, the equations treating the barrier as a laminate of two diffusion layers with a membrane between adequately describe both the stationary- and nonstationary-state processes. No viable alternative hypotheses appear available to account for the observed behavior. Thus, the conclusion is inescapable that diffusion layers are an integral and often very significant part of the barrier. This, of course, strictly applies to permeation that takes place from a solution, through a membrane, and into a second solution of lesser concentration.

Theoretical Analysis of Solubility-Limited Diffusion Layer Membrane Model—The need for a differentiable solubility function for the alkyl *p*-aminobenzoates and the resulting fit to a second-order equation have been described. This expression, when combined with Eqs. 10 and 11, leads to the following modified forms of Eqs. 15 and 16, respectively:

$$\log F_n^s = \log S_0 + \log (PC)_0 + n(\pi - \delta) - \epsilon n^2 - \log [R_{AQ}(PC)_0 10^{\pi n} + R_M] \qquad \text{(Eq. 27)}$$

and:

$$\frac{d(\log F_n^s)}{dn} = \pi - \delta - 2\epsilon n - \frac{R_{AQ}(PC)_0 \pi 10^{\pi n}}{R_{AQ}(PC)_0 10^{\pi n} + R_M} \qquad \text{(Eq. 28)}$$

Both Eqs. 27 and 28 (or their counterparts for the simpler solubility relationship) are in suitable form for computer programming. The smooth curve in Fig. 7 is a computer-drawn line for the logarithm of the steady-state flux against carbon number. The second-order solubility relationship and experimental parameters actually obtained in the diffusional runs were used to generate the curve. The values of h_M, Σh_{AQ}, π, and $(PC)_0$ were (specifically) 0.0476 cm., 0.0188 cm., 0.540, and 0.027, respectively. Also shown on this plot are the actual experimental fluxes (data) and calculated fluxes using the above experimental parameters and the actual raw solubility data. The latter approximation is virtually a perfect fit to the experimental. The computer approximation is also quite good; deviations are at their greatest where the solubility approximation

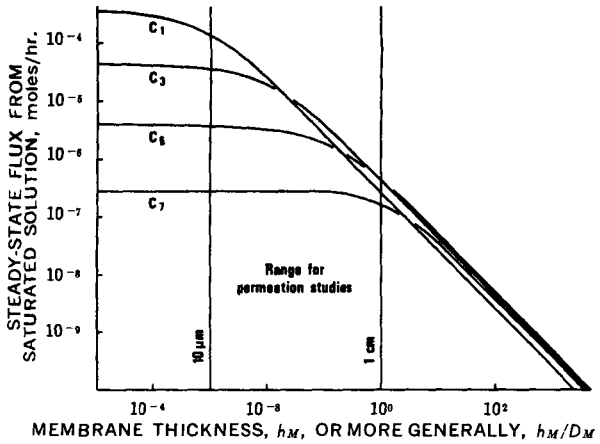

Figure 8—*Computer curves for flux for the odd chain length alkyl* p*-aminobenzoates as a function of membrane thickness (or membrane resistance). Curves labeled* C_1, C_3, C_5, *and* C_7 *are for the methyl, propyl, pentyl, and heptyl derivatives, respectively. All other diffusional parameters were constant (see text). The rank order in the membrane control region is determined by the product of the respective solubilities and partition coefficients. In this case, the computer-generated solubility is used.*

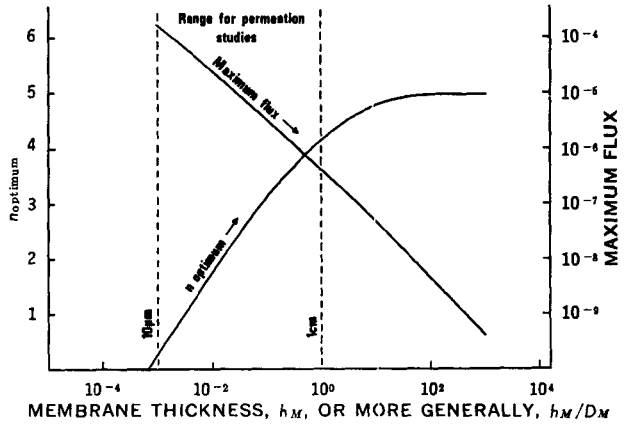

Figure 10—*Computer-generated plots of* $n_{optimum}$ *and flux thereat as a function of membrane thickness,* h_M *(or membrane resistance), using diffusional parameters reported in the text. In the accessible experimental range,* $n_{optimum}$ *is virtually directly dependent on the log of the membrane thickness for the alkyl* p*-aminobenzoates.*

was poorest; specifically, this was at the break in the curve at the butyl ester.

The computer program makes it possible to assess the effect of a single variable on the shape of the steady-state flux profile. Since π and δ (ϵ can be excluded since it is not part of the general case) do not exhibit wide extremes of values and are generally beyond experimental control, these parameters are treated as constants in the computer analysis. However, the values of h_M and Σh_{AQ} can vary widely, depending on the experimental design. Furthermore, since the theory is general, the program is applicable to other membranes, other solvents, and other experimental situations in which the values of D_M, D_{AQ}, S_0, and $(PC)_0$ may range over many orders of magnitude. Fortunately, most, and in some cases all, of these parameters are experimentally determinable. For the very reason that this approach is applicable to a diversity of membrane permeation systems, the effect on the steady-state flux curve resulting from variations in each of these parameters is of more than just theoretical interest.

Laminate thicknesses and the diffusivities therein appear as the resistance ratios, R_{AQ} and R_M, in the permeability equations. Increases in thickness or decreases in diffusivity or vice versa will have the same qualitative effect on the steady-state flux profile. By choosing a specific membrane and solvent, the effect can be limited to laminal thickness alone. The result of increasing h_M (or, more generally, h_M/D_M) is illustrated in Fig. 8 where the logarithm of the steady-state flux from saturated solutions for each of the odd chain length alkyl aminobenzoates is plotted against these parameters. For illustrative purposes, thicknesses on this plot range from about 100 Å, approximately mammalian cell membrane dimensions, to 100 m. or the length of a football field. Workable dimensional extremes, 10 μm. to 1 cm., are indicated on the plot (the membrane must be of some minimum thickness to be handled). The plateau for each ester corresponds to the region where the permeation of that ester is in diffusion layer control. The down slope has a value of −1 corresponding to membrane control where flux is proportional to the reciprocal of thickness. Within the normal experimental range of membrane thickness for dimethylpolysiloxane membranes (for the alkyl *p*-aminobenzoates), the methyl ester is totally in membrane control and the heptyl ester is completely within diffusion layer control. The propyl and pentyl esters exhibit a change in dependency on the low and high ends of the span, respectively. The ethyl, butyl, and hexyl esters could have been similarly treated, but this would have complicated the plot without providing substantial additional information. When comparing different membranes, the x axis should be thought of as R_M rather than just thickness alone. For most other membranes, the location of the 10-μm. and 1-cm. markers would be shifted markedly to the right since diffusivities within dimethylpolysiloxane are very large relative to other materials. It is possible, for instance, that the permeation of something like polyethylene by heptyl *p*-aminobenzoate would be primarily in membrane control at practical membrane thicknesses due to an orders of magnitude smaller diffusion coefficient.

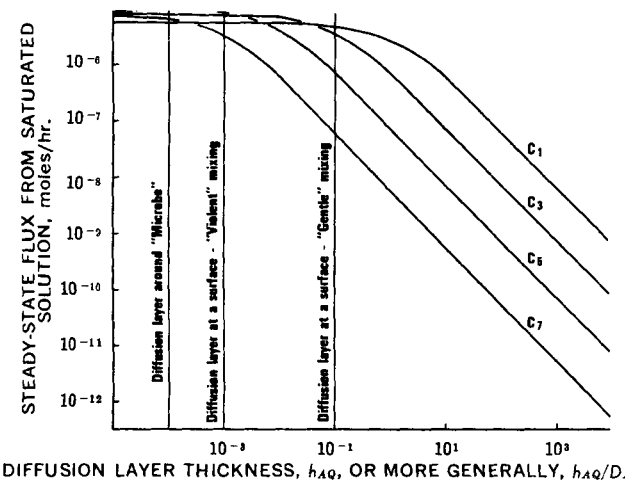

Figure 9—*Computer curves for flux for the odd chain length esters as a function of diffusion layer thickness,* h_{AQ} *(or diffusion layer resistance). The curves are based on a membrane thickness of 0.0476 cm. and diffusional parameters reported in the text. The methyl, propyl, pentyl, and heptyl derivatives are designated by* C_1, C_3, C_5, *and* C_7, *respectively.*

Changing the thickness of the diffusion layer (or, generally, the value of R_{AQ}) produces a similar set of steady-state flux profiles (Fig. 9). The order of esters on the down slope is the same as on the plateau of the previous plot since both regions represent diffusion layer control. In this situation, as the diffusion layer thickness (resistance) decreases, the flux increases until transition to membrane control is accomplished. At this point the flux plateaus. This plot indicates that for infinitesimally thin diffusion layers, the maximum flux is comparable for all esters. In other words, the effect of partitioning is not shunted out and, since the product of $(PC) \times S$ varies only slightly through this span, the fluxes are relatively constant. This would not be the general case, because the value of δ is usually significantly greater than π; thus the shortest ester would have the largest flux, with the log (flux) decreasing decrementally as chain length is increased. Throughout the experimentally utilizable range, 10^{-3}–1 cm., both the pentyl and heptyl compounds are in diffusion layer control. The methyl and propyl esters both show transitions in this region.

If the carbon number for maximum penetration is plotted against the logarithm of h_M (Fig. 10), it is found that the apex of the flux

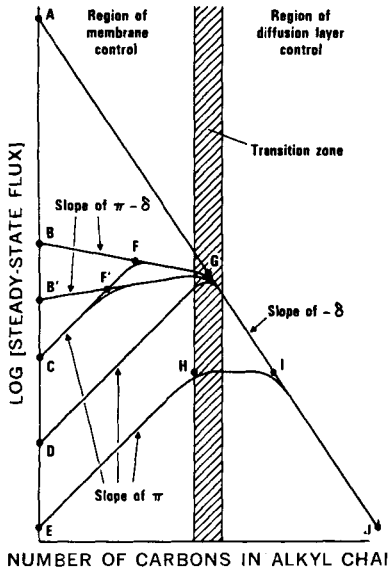

Figure 11—*Hypothetical plot illustrating the various possible flux dependencies for a homologous series as a function of concentration in a system fixed with regard to diffusional parameters. Where biological activity parallels flux, the plot can be regarded as a series of structure–activity profiles.*

profile is sensitive to the thickness of the membrane. Here again the more general treatment would be for membrane resistance, R_M. In the dimethylpolysiloxane system, the carbon number of maximum flux increases by about one carbon for a 10-fold change in R_M and varies from about 1 to a little over 4 in the tractable thickness region. Therefore, cognizance must be given to the degree of parallelism between the resistances of the biological membrane and its "model membrane counterpart" in the simulation of biological phenomena to produce *in vitro* results in agreement with *in vivo* behavior.

The logarithm of F^s at the apex of the curve similarly changes with increasing membrane resistance or, for fixed diffusivity, increasing membrane thickness. A steady decline is observed (Fig. 10). Thus, the more resistance encountered within the membrane, the less is the penetration rate of the ester with maximum throughput. The impenetrability of the skin which, by biological standards, is a thick membrane of very low diffusivity can be explained on this basis. Although trends are general, the data in Figs. 8–10 are specifically for the alkyl *p*-aminobenzoate permeation of the dimethylpolysiloxane–water barrier.

Some features of the solubility-limited diffusion layer membrane model are summarized in Fig. 11. This figure is essentially a plot of the various flux profiles one might expect to find for a given homologous series of diffusants in a given permeation system as a function of concentration. The line A to J has a slope of $-\delta$ and may be thought of as the flux curve for saturated solutions using an infinitely thin membrane. For a fixed membrane system with practical dimensions, this line is theoretical from point A to point G, the membrane control region. Line AJ is drawn for linear solubility dependency, as defined in Eq. 12, over the entire range. Obviously, this line would be kinked for the alkyl *p*-aminobenzoates due to the change in solubility dependency at butyl.

Curves BGJ and B'GJ (Fig. 11) are the profiles to be expected from saturated solutions when a membrane of finite thickness is employed. These are drawn with negative and positive slopes to represent the cases where $\pi < \delta$ (BFG) and where $\pi > \delta$ (B'FG). The mathematical expression characterizing these profiles is Eq. 13. It can be seen that as n approaches zero, the intercept on the y axis approaches a value of $S_0(PC)_0/R_M$ (Eq. 15).

Points C, D, and E are starting concentrations less than saturation, which have also been sequentially dropped with respect to one another. Collectively the curves illustrate the different situations one might observe when working on a normalized concentration (isomolar) basis. Curve CFGJ (or CF'GJ) represents the situation where the selected concentration is sufficiently close to the saturation (flux-limiting) line so as to intersect with this line while the whole process is still in membrane control. It has three sections and these, from left to right, have slopes of π, $\pi - \delta$, and, finally, when diffusion layer control is attained, $-\delta$. The value of point C is equal to $C_c(PC)_0/R_M$.

Curve DGJ has only two sections because the attainment of diffusion control and the attainment of solubility-limited flux occur together. This profile initially increases with a slope of π and, as in all the curves, it declines with a slope of $-\delta$. When the attainment of diffusion layer control occurs at concentrations significantly less than saturation, another profile is observed, curve EHIJ. The plateau region has a height of C_E/R_{AQ}. The y intercepts of curves DGJ and EHIJ are $C_D(PC)_0/R_M$ and $C_E(PC)_0/R_M$, respectively. The fixed concentration curves illustrate several points:

1. The steady-state flux or any phenomenon directly dependent thereupon increases uniformly with a slope of π until it intersects with the solubility-limiting line.

2. Since the solubility-limiting line is intersected at higher and higher values of n as concentration is reduced, the chain length of maximum steady-state flux (or maximum biological response if the biological phenomenon is permeation dependent) is sensitive to the concentration chosen, particularly in membrane control. Therefore, the choice of concentrations can cause discrepancies between biological data (point of maximum response, *etc.*) and *in vitro* studies aimed at correlating them with a physical model, even if all of the biological system's diffusional parameters were correctly assigned.

For a given system (membrane and solvent) and a particular homologous series, S_0 and $(PC)_0$ are true constants. Often it is desirable to compare related homologous series in an otherwise fixed diffusional system, be it a microorganism or a membrane. The effect of the introduction of a hydroxyl group into some basic molecule to create a new hydroxylated series provides an illustrative example. For each corresponding member of the new series, there will be an increased polarity or a depression of the membrane–water partition coefficient, usually by a reasonably predictable amount (23). This functional group will also impart an increase in aqueous solubility to each member of the new series relative to that of its nonhydroxylated counterpart. Derivatization may also lead to a slight change in the value of δ. The increase in solubility and decrease in partition coefficient will likely be of similar magnitude. If this is assumed to be the case, then the net effect on steady-state flux profiles similar to curves CFGJ or DGJ (Fig. 11) for the two

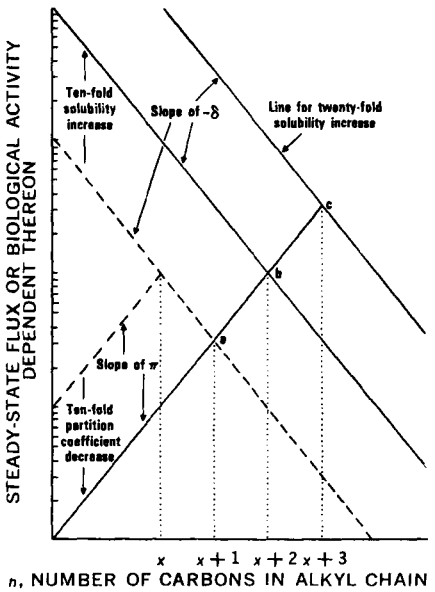

Figure 12—*Expected effect of increasing polarity (hydroxyl addition) on the flux profiles of parent (dashed lines) and derivative (solid lines) series. When the solubility and partition coefficient changes are offsetting, there is a shift in the maximum carbon number to* x + 2 *but little change in maximum flux. When there is no increase in solubility or a disproportionate increase, the flux profile is still shifted to the right and is accompanied by significant changes in maximum flux.*

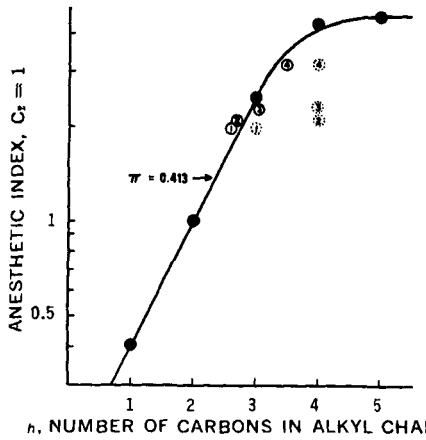

Figure 13—*Data of Adams* et al. *(38) for the anesthetic index (ethyl equal to 1) of alkyl* p-*aminobenzoates as a function of chain length. The filled circles, ●, are for the normal esters. The solid numbered circles are for the branched esters (1, isopropyl; 2,* tert-*butyl; 3,* sec-*butyl; and 4, isobutyl) which have been adjusted from their original positions (dotted numbered circles) for the effects of branching.*

series will be a shift of the peak to a higher carbon number without a significant change in peak height. If the partition coefficient and solubility change are not of comparable magnitude or if there is a significant change in δ, the magnitude of the optimized steady-state flux will also be affected. These features are illustrated in Fig. 12. The dashed curve represents the logarithm of the flux profile from isomolar solutions for the basic series. The hydroxyl incorporation results in a decrease in partition coefficient which directly affects and depresses the membrane control portion of the curve to the lower solid line. The solubility increase produces an upward shift in the diffusion layer control line (infinitely thin membrane, saturated solutions) to the upper solid line. The intersection of the dotted and dashed lines is the carbon number of optimum flux for the new series, and this occurs at larger carbon numbers. In Case b, the peak heights are comparable because solubility and partition coefficient changes were drawn to similar magnitudes. The exact reversal of this trend is expected for decreases in relative polarity; *i.e.*, the hydroxylated series could have been chosen as the reference point. If the logarithm of the actual membrane–water partition coefficient were used in place of n, these two curves would merge. However, for most systems, membrane–water partition coefficients are not known. It is common practice to use partition coefficients

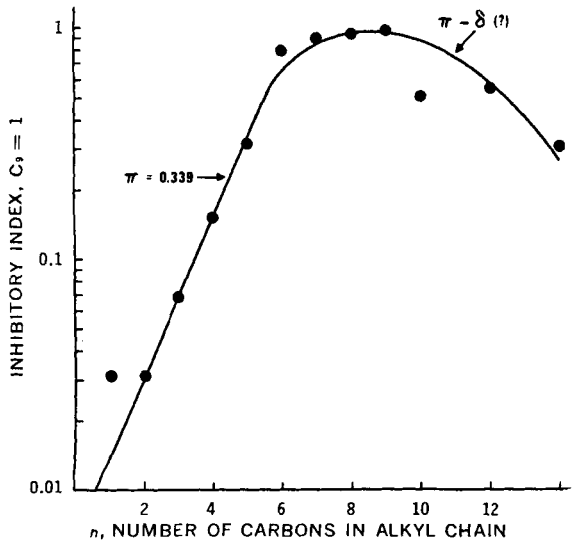

Figure 14—*Data of Kakemi* et al. *(42) for the minimum inhibitory concentration of a series of alkyl* o-*hydroxy-*p-*aminobenzoates against* Myc. tuberculosis. *The data are plotted as the log [inhibitory index] (nonyl equal to 1) against chain length.*

obtained in some arbitrarily chosen immiscible solvents in their stead, but this can be misleading if, and to the extent that, *in vitro* partitioning fails to approximate partitioning in the permeation process.

During this study, an extensive perusal of the diffusional literature was made. Included were biological response data dependent upon a permeation step. Examples fitting each prototype curve were found; some of these are detailed here. The relationships of antibacterial activity to chain length in several phenolic series (phenol coefficients) seem to be cases represented by curve CFG in Fig. 11 (34–36). The addition of sodium hydroxide, depressing the concentration of free phenol, or of alcohol, depressing the solvent–bacteria partition coefficient, each leads to higher values for optimized n, consistent with the way the model operates. Also consistent is the intersection with the solubility-limiting line while still in membrane control (the down slopes are very shallow), because diffusion layer thickness would be on the order of the thickness of the microorganism itself (37) and thus would be roughly 100 times thinner than those generated against a stationary surface. The following examples are more extensively treated. The anesthetic index data of Adams *et al.* (38) are a classical example of curve EHI, shown in Fig. 11.

Biological Data Viewed from the Solubility-Limited Membrane Diffusion Layer Model—There is a plethora of information in the literature, biological and otherwise, which has been interpreted without cognizance of the presence of diffusion layers and their potentially flux-limiting role. The classical membrane control model has led to the postulation of an adsorption mechanism where it was not necessary (39, 40), to the incorrect assignment of slopes (41), and to confusion and somewhat contradictory results for seemingly identical experiments run in different laboratories (34–36). With the strict membrane control model, it is impossible to interpret the "biological parabola" on a rational physical–chemical basis as a permeation phenomenon alone. In these instances, invocation of the solubility-limited, membrane diffusion layer control model would have facilitated interpretation or provided optional interpretation and may have led the authors to different conclusions.

In 1926, Adams *et al.* (38) published a paper relating alkyl chain length of alkyl *p*-aminobenzoates to their anesthetic potency. Ten compounds were studied, including the normal alkyl esters from methyl to pentyl. The time it took goldfish to become "comatose" and lose their ability to respond to the painful pressure of a glass rod on their tails while in tanks of fixed drug concentration was used as the biological end-point. This was found to be a reliable, reproducible measurement. Clearly this response is dependent to a large extent on a membrane permeation (absorption) step. The reported anesthetic indexes are plotted against carbon number in Fig. 13. The filled circles are for the straight-chain esters, the numbered open circles are for the branched compounds. The carbon numbers (logarithm of the partition coefficient) for the latter were adjusted downward by a factor of 0.85 per branch to account for the effect of branching (23). The dotted, numbered ghosts indicate the original positions of the branched esters. By considering only the normal esters, it can be seen that the index increases logarithmically up to propyl and then levels off, with the pentyl ester appearing to be on the presumed plateau. The curve is identical in form to the concentration-normalized plot for silastic membranes (Fig. 6) and to theoretical curve EHI in Fig. 11. After adjusting for branching, the other esters also fit on this curve. A suitable explanation for the trend is that absorption of the shorter chain esters was controlled by a membrane gradient (in the gills of the fish ?), with a shift to diffusion layer control at longer chain length. When these data were treated by Zahradnik (41) years later, a least-squares line was drawn through the points as they lay, giving a false impression of the magnitude of the index increase as a function of chain length. Other observations of Adams *et al.* (38) are consistent with a transition to solubility limitations and diffusion layer control, particularly the trend in recovery time of the goldfish when returned to fresh water. These were of short duration (less than 5 min.) for the esters assumed to be absorbed and desorbed through a membrane gradient. Recovery times for the longer esters were protracted and increased with increasing chain length, the pentyl ester being slower than the normal butyl ester, *etc.* The gradient in the diffusion layer (diffusion layer control) determining the rate of desorption should become shallower and shallower with increasing chain length, and thus the lengthened recovery times are expected. The π value taken from the membrane control region (slope of line through the points)

is 0.413, which is equivalent to a 2.59 increase in anesthetic index per methylene unit in this region[10].

The data of Kakemi *et al.* (42) for the minimum inhibitory concentrations of several series of alkyl *o*-hydroxy-*p*-aminobenzoates on *Mycobacterium tuberculosis* may be similarly treated. Such studies are obviously also dependent in part on relative membrane permeability, in this case penetration through the bacterial cell wall. The inhibitory indexes for the normal alkyl esters calculated by setting nonyl equal to 1.0 are shown in Fig. 14. A curve is obtained which is strikingly similar to theoretical curve CFG, Fig. 11. It rises rapidly with a slope (π value) of 0.339, corresponding to a 2.18 increase in activity per methylene addition. The curve peaks at nonyl and then declines gradually. These data may be rationalized if transport into the cells is solely dependent on the concentration of the neutral, zwitterionic species. Eventually the solubility of this species for one of the alkyl esters would be reached, resulting in an intersection with the solubility-limited flux line. Thereafter, it would decline with a slope of $\pi - \delta$ until diffusion layer control is attained. As pointed out previously when discussing phenolic activities, the intersection with the solubility-limiting line is in the membrane control region since the diffusion layer is extremely thin (37). Another interesting feature of these data is that the apex for the ω-hydroxyalkyl series is at a longer chain length than the normal alkyl series. This is an expected result of increasing polarity. Since the peak in potency of the ω-hydroxyalkyls is higher than that for straight-chain series, it is likely that the additional hydroxyl also increases the intrinsic activity.

A series of studies (39, 40, 43) on barbiturate absorption through the intestine of the rat led to the conclusions that either the process is controlled by adsorption onto mucosal tissue or that pores exist within the membrane. Examination of the structures and solubilities of these compounds suggests that partitioning into a semipolar membrane would be favored; *i.e.*, the ether–water partition coefficient of barbital, the lowest member of the series, is 3.7 based on the ratio of solubility in these two solvents (44). Thus the biological partition coefficients could be considerably greater than one. Assuming this to be true, then the data are explicable on the basis of diffusion layer control of the absorption process. The pH dependency implicit in the pH-partition hypothesis would still be observed if only the neutral species was absorbed. The partitioning dependency, on the other hand, should break down as the flux is being controlled by a gradient essentially in the diffusion layer. These features are in keeping with the experimental observations. Since the diffusion layer thickness and concentration were established and held constant by experimental design, the steady-state flux should only be dependent on the aqueous diffusivity, D_{AQ}. Slight differences in D_{AQ} between the oxy, *n*-methyl, and thio series likely account for the slight differences in permeation rates from series to series. Further support for this mechanism is derived from the fact that penetration through the rat gastric mucosa (43), a more formidable barrier by all evidence gathered to date, does show a partitioning dependency.

The membrane diffusion layer model leads to an alternative interpretation of recent data of Mayerson and Gibaldi (45, 46) on the inhibition by glucose, *etc.*, of the absorption of riboflavin, salicylate, and sulfanilamide. If the absorption is in diffusion layer control, then one of the mechanisms of these authors is indeed plausible, *i.e.*, that the retardation is due to thickening of the cell resulting in a diminution of the diffusion layer gradient. Implicit here is the fact that the cell contents, protoplasm, are part of the aqueous barrier. However, in our opinion, it is not likely that all three of these compounds would be absorbed by this mechanism; rather, the principal barrier is likely within the cell wall. If a membrane gradient is controlling, the suppression of flux by some sugars and ions cannot be attributable to changes in the aqueous regions of the cell but must be due to fundamental change within the cell membrane. This is at least conceivable since the causative agents are actively absorbed and require mobilization of special membranous proteins for their transfer. According to this line of reasoning, the decreases in permeability indicate that the active transport process is accompanied by changes that make the membrane more rigid or impermeable (possible dehydration, considering the swelling of the cell). Thus, the water imbibement can be concurrent with the absorption without being causative of the permeability decrease.

In summary, a new diffusional model incorporating features of the classical membrane treatment, newer treatments which include diffusion layer involvement, and solubility restrictions has been conceived and developed. Experimental evidence in an *in vitro* system indicates that the model is extremely sound in its construction. Subsequently, a theoretical analysis of the model has demonstrated its very broad applicability to a number of membrane transport problems, and an analysis of some selected literature data has basically substantiated this view. These treatments will be expanded in future reports. In the literature cases cited, the solubility-limiting diffusion layer membrane model provides alternative—not absolute—interpretations. In general, this model allows for collation of so much seemingly unreconcilable data that it is possible to conclude that most processes in which a barrier passage is influential can be resolved into one or another of the theoretical cases presented in Fig. 11, depending, of course, on the experimental design.

[10] This value is in good agreement with the biological π values found by N. F. Ho and W. I. Higuchi for buccal absorption and by S. H. Yalkowsky and G. L. Flynn for a multifarious group of biological phenomena (manuscript in preparation).

GLOSSARY OF TERMS

A = cross-sectional diffusional area
C = concentration
D_{AQ} = permeant diffusivity in aqueous (solvent) barrier region
D_M = permeant diffusivity in the membrane
d = superscript referring to donor phase
δ = change in aqueous solubility within a homologous series per methylene unit (on a logarithmic scale)
δ_1 = logarithmic change in solubility of alkyl *p*-aminobenzoates per —CH_2— from methyl to butyl
δ_2 = logarithmic change in solubility of alkyl *p*-aminobenzoates per —CH_2— from butyl to dodecyl
ϵ = curve fitting second-order solubility factor
F = steady-state flux
F^s = steady-state flux from saturated solution
F^c = steady-state flux from solution of concentration C
F_n^s = steady-state flux from saturated solution, nth homolog
$F_n^{c=1}$ = steady-state flux from concentration-normalized solution, nth homolog
h_{AQ} = thickness of an individual diffusion layer
h_M = thickness of membrane
K = adsorption constant for esters on membrane filler
M = mass
n = length of alkyl chain
$n_{optimum}$ = chain length of maximum steady-state flux
(PC) = partition coefficient
$(PC)_n$ = partition coefficient for nth homolog
$(PC)_0$ = imaginary extrapolated partition coefficient of the homolog with zero chain length
π = logarithmic change in partition coefficient per methylene unit
R_T = total diffusional resistance
R_{AQ} = diffusional resistance encountered in the solvent
R_M = diffusional resistance encountered in membrane
r = superscript referring to receptor phase
S = solubility
S_0 = extrapolated solubility of imaginary homolog of zero alkyl chain length
S_n = solubility of nth homolog
t = time
t_L = lag time
V_2 = volume fraction of filler in membrane

REFERENCES

(1) R. G. Stehle and W. I. Higuchi, *J. Pharm. Sci.*, **56**, 1367 (1967).

(2) R. G. Stehle, Ph.D. thesis, University of Michigan, Ann Arbor, Mich., 1970.

(3) N. F. Ho and W. I. Higuchi, *J. Pharm. Sci.*, **60**, 537(1971).

(4) R. M. Barrer, J. A. Barrie, and N. K. Raman, *Polymer*, **3**, 595(1962).

(5) R. M. Barrer and H. T. Chio, *J. Polym. Sci., Part C*, **1965**, 111.

(6) E. R. Garrett and P. B. Chemburkar, *J. Pharm. Sci.*, **57**, 944(1968).
(7) *Ibid.*, **57**, 949(1968).
(8) *Ibid.*, **57**, 1401(1968).
(9) M. Nakano and N. K. Patel, *J. Pharm. Sci.*, **59**, 79(1970).
(10) J. Haleblian, R. Runkel, N. Mueller, J. Christopherson, and K. Ng, *ibid.*, **60**, 541(1971).
(11) C. F. Most, *J. Appl. Polym. Sci.*, **14**, 1019(1970).
(12) G. L. Flynn and T. J. Roseman, *J. Pharm. Sci.*, **60**, 1788 (1971).
(13) G. L. Flynn and R. W. Smith, *ibid.*, **61**, 61(1972).
(14) T. J. Roseman and W. I. Higuchi, *ibid.*, **59**, 353(1970).
(15) T. J. Roseman, *ibid.*, **61**, 46(1972).
(16) T. Higuchi, *ibid.*, **52**, 1145(1963).
(17) B. J. Zwolinski, H. Eyring, and C. E. Reese, *J. Phys. Chem.*, **53**, 1426(1949).
(18) R. E. Beck and J. S. Schultz, *Science*, **170**, 1302(1970).
(19) J. Dainty and C. R. House, *J. Physiol.*, **182**, 66(1966).
(20) A. W. Cuthbert and Y. Dunant, *Brit. J. Pharmacol.*, **40**, 508(1970).
(21) G. L. Flynn and E. W. Smith, *J. Pharm. Sci.*, **60**, 1713 (1971).
(22) H. C. Brill, *J. Amer. Chem. Soc.*, **43**, 1320(1921).
(23) G. L. Flynn, *J. Pharm. Sci.*, **60**, 345(1971).
(24) T. Higuchi and S. S. Davis, *ibid.*, **59**, 1376(1970).
(25) G. Saracco and E. S. Marchetti, *Ann. Chim.*, **48**, 1357(1958).
(26) H. A. Daynes, *Proc. Roy. Soc., Ser. A*, **97**, 286(1920).
(27) R. M. Barrer, *Trans. Faraday Soc.*, **35**, 628(1939).
(28) K. F. Finger, A. P. Lemberger, T. Higuchi, L. W. Busse, and D. E. Wurster, *J. Amer. Pharm. Ass., Sci. Ed.*, **49**, 569(1960).
(29) W. I. Higuchi and T. Higuchi, *ibid.*, **49**, 598(1960).
(30) G. L. Flynn, O. S. Carpenter, and S. H. Yalkowsky, *J. Pharm. Sci.*, **61**, 312(1972).
(31) S. H. Yalkowsky, G. L. Flynn, and T. G. Slunick, *ibid.*, **61**, 852(1972).
(32) I. D. Robb, *Austr. J. Chem.*, **19**, 2281(1966).
(33) J. J. Kipling, "Adsorption from Solutions of Nonelectrolytes," Academic, New York, N. Y., 1965, pp. 179–187.
(34) E. G. Klarmann, V. A. Shternov, and W. L. Gates, *J. Lab. Clin. Med.*, **20**, 40(1934).
(35) J. B. Niederl, V. Niederl, S. Shapiro, and M. E. McGreal, *J. Amer. Chem. Soc.*, **59**, 1113(1937).
(36) R. R. Read and E. Miller, *ibid.*, **54**, 1195(1932).
(37) W. I. Higuchi, *J. Pharm. Sci.*, **56**, 315(1967).
(38) R. Adams, E. K. Rideal, W. B. Burnett, R. L. Jenkins, and E. E. Dreger, *J. Amer. Chem. Soc.*, **48**, 1758(1926).
(39) K. Kakemi, T. Arita, R. Hori, and R. Konishi, *Chem. Pharm. Bull.*, **15**, 1883(1967).
(40) K. Kakemi, T. Arita, R. Hori, R. Konishi, and K. Nishimura, *ibid.*, **17**, 248(1969).
(41) R. Zahradnik, *Arch. Int. Pharmacodyn. Ther.*, **135**, 311 (1962).
(42) K. Kakemi, T. Arita, S. Kitazawa, M. Kawamura, and H. Takenaka, *Chem. Pharm. Bull.*, **15**, 1819(1967).
(43) K. Kakemi, T. Arita, R. Hori, and R. Konishi, *ibid.*, **15**, 1534(1967).
(44) "The Merck Index," 7th ed., Merck & Co., Rahway, N. J., 1960, p. 119.
(45) M. Mayerson and M. Gibaldi, *J. Pharm. Sci.*, **58**, 1429(1969).
(46) *Ibid.*, **60**, 225(1971).

ACKNOWLEDGMENTS AND ADDRESSES

Received October 29, 1971, from the *Pharmacy Research Unit, The Upjohn Company, Kalamazoo, MI 49001*

Accepted for publication February 2, 1972.

The authors express their indebtedness to Mr. R. W. Smith for technical assistance and Dr. M. A. Rebenstorf who performed the hydrogenations converting nitro compounds to amines. Dr. W. Morozowich and Dr. R. G. Stehle's constructive criticisms and comments are acknowledged, as is the critical review of the manuscript by Mr. E. L. Rowe. Thanks are also extended to Mr. O. S. Carpenter for assisting in the computer analyses. (All mentioned are personnel of The Upjohn Co.) The authors would also like to thank the reviewer for his very conscientious efforts on their behalf.

▲ To whom inquiries should be directed.

Importance of Chain Length on Physicochemical and Crystalline Properties of Organic Homologs

S. H. YALKOWSKY▲, G. L. FLYNN, and T. G. SLUNICK

Abstract □ It has been observed that certain physical properties of normal alkyl *p*-aminobenzoates (*i.e.*, their melting behavior and their solubilities in water, silicone oil, and hexane) exhibit an unusual dependency upon chain length. Each property is characterized by a definite break in the chain length profile about the butyl ester. However, the silicone oil–water and hexane–water partition coefficients of these esters show a regular increase with chain length extending over many orders of magnitude. The overall behavior of these homologs is attributed to basic difference in the crystal lattices of short (≤four carbons) and long (≥four carbons) homologs. X-ray patterns and thermal data were obtained and are supportive of this conclusion. As an additional verification, the hexane solubility of each compound was calculated by Scatchard–Hildebrand theory using the thermal data and empirically estimated solubility parameters. Agreement between calculated and experimental values is excellent. Because of relationships drawn for the influence of chain length on solubility and relative solubility (partition coefficients), these experiments also indicate a convenient method of estimating congeneric solubilities in other solvents.

Keyphrases □ Alkyl *p*-aminobenzoates—effect of chain length on melting point, solubilities, partition coefficients, crystalline properties □ Homologous alkyl series, *p*-aminobenzoates—effect of chain length on melting point, solubilities, partition coefficients, crystalline properties □ Chain length effect—melting point, solubilities, partition coefficients, and crystalline properties of alkyl *p*-aminobenzoates □ Structure–activity relationships—effect of alkyl chain length on physicochemical and crystalline properties, *p*-aminobenzoate esters

The importance of a drug's physical–chemical properties in determining its biological and pharmaceutical characteristics has long been recognized. Of particular importance are the aqueous solubility and the partition coefficient which are the major determinants of a drug's dissolution, distribution, and availability. An under-